ELSEVIER

International Journal of Mass Spectrometry 212 (2001) 301–325

www.elsevier.com/locate/ijms

Relative and absolute bond dissociation energies of sodium cation complexes determined using competitive collision-induced dissociation experiments

Jay C. Amicangelo, P. B. Armentrout*

Department of Chemistry, University of Utah, Salt Lake City, Utah 84112

Received 27 April 2001; accepted 9 July 2001

Abstract

Absolute $L_1Na^+–L_2$ and relative $Na^+–L$ bond dissociation energies are determined experimentally by competitive collision-induced dissociation of $L_1Na^+L_2$ complexes with xenon in a guided ion beam mass spectrometer. The ligands examined include H_2O, C_6H_6, CH_3OH, CH_3OCH_3, NH_3, and C_2H_5OH, which cover a range in Na^+ affinities of only 20 kJ/mol. Dissociation cross sections for formation of $Na^+L_1 + L_2$ and $Na^+L_2 + L_1$ are simultaneously analyzed with a model that uses statistical theory to predict the energy dependent branching ratio. The use of independent and common scaling factors for each channel in this analysis is evaluated and discussed, as is the importance of properly handling ligand internal rotors. The cross section thresholds thus determined are interpreted to yield the 0 K $L_1Na^+–L_2$ bond dissociation energies and the relative 0 K $Na^+–L$ binding affinities. The relative binding affinities are converted to absolute 0 K $Na^+–L$ binding energies by using the absolute bond energy for $Na^+–NH_3$, determined previously in our laboratory, as an anchor value. Comparisons are made to previous experimental and theoretical $Na^+–L$ thermochemistry from several sources. The absolute $L_1Na^+–L_2$ bond dissociation energies were also calculated using ab initio theory at the MP2(full)/6-311+G(2d,2p)//MP2(full)/6-31G* level (corrected for zero-point energies and basis set superposition errors) and are in good agreement with the experimentally determined values. (Int J Mass Spectrom 212 (2001) 301–325) © 2001 Elsevier Science B.V.

Keywords: Guided ion beam mass spectrometry; Competitive collision-induced dissociation; Sodium complexes; Bond dissociation energies

1. Introduction

Recently, there have been several reviews and comprehensive studies regarding the gas-phase binding energetics (both experimental and theoretical) of sodium cations with small organic molecules [1–4]. The interest in this topic is a result of the importance of the sodium cation in biological systems [5], as well as the increased use of gas-phase sodium cations in biological applications of mass spectrometry [6]. An accurate, absolute sodium cation affinity scale is essential for a complete understanding of the participation and binding characteristics of sodium ions in these systems.

The most extensive experimental and theoretical $Na^+–L$ studies have been performed in the laboratories of Castleman and coworkers [7–11], McMahon,

* Corresponding author. E-mail: armentrout@chemistry.utah.edu

In honor of Graham Cooks on his 60th birthday and in thanks for his many contributions across the field of mass spectrometry.

PII S1387-3806(01)00494-8

Ohanessian and coworkers [1,2], Rodgers and coworkers [12–15], and in our own laboratory [3,4,16–20]. In general, there is fairly good agreement between the absolute Na^+–L bond dissociation energies (BDEs) determined in our laboratory by collision-induced dissociation (CID) experiments and those determined using other experimental techniques [3]. However, a close examination of the data reveals notable differences between our results and those reported in the literature. For example, high-pressure mass spectrometry studies [10,11,21], and more recent Fourier transform ion cyclotron resonance (FTICR) experiments [2] find that the binding energy of Na^+ to benzene is greater than that to water [22], whereas our CID studies indicate that Na^+ is more strongly bound to water [16] than to benzene [3,20]. Theory at several levels, on the other hand, predict the bond energies for these two ligands with the sodium cation to be essentially equivalent [1,3]. There were also some discrepancies between the trends in the absolute BDEs for the methanol, ethanol, and dimethyl ether complexes determined using CID and FTICR experiments. The present experiments were undertaken in an effort to determine more accurate relative and absolute Na^+–L BDEs for the ligands in question by examining CID experiments on doubly-ligated complexes of the sodium cation, $L_1Na^+L_2$, and using our recently developed data analysis model that explicitly considers competitive dissociation [23].

In this work, we perform CID experiments on $L_1Na^+L_2$ complexes, where L_1 and L_2 include water, benzene, methanol, dimethyl ether, ammonia, and ethanol, using a tandem guided ion beam mass spectrometer. Simultaneous analysis of the competitive dissociation cross sections is accomplished using independent and common scaling factors for the two channels and the preferred treatment is evaluated in some detail. Explicit handling of internal rotors that are constrained upon complexation is found to be an important consideration. The ultimate threshold results are converted to absolute 0 K L_1Na^+–L_2 bond dissociation energies and relative 0 K Na^+–L binding affinities. The relative Na^+–L binding affinities are converted to absolute bond energies using an absolute anchor value: the BDE of Na^+–NH_3 determined previously in our laboratory [3]. The present absolute Na^+–L BDEs are compared to available literature thermochemistry (experiment and theory). The absolute L_1Na^+–L_2 bond dissociation energies were also calculated using ab initio theory at the MP2(full)/6-311+G(2d,2p)//MP2(full)/6-31G* level and are compared with the experimentally determined values.

2. Experimental methods

2.1. General

The guided ion beam instrument on which these experiments were performed has been described in detail previously [24,25], except for a modification of the octopole ion guide, the experimental details of which are described elsewhere [26]. Briefly, ions are created in a dc-discharge/flow tube ion source, as described below. After extraction from the source, the ions are accelerated and passed through a magnetic sector for mass analysis. The mass-selected ions are then decelerated to the desired kinetic energy and focused into an octopole ion beam guide. This device uses radio-frequency (rf) electric fields to trap the ions in the radial direction and ensure complete collection of reactant and product ions [27,28]. The current arrangement consists of two consecutive octopole ion guides, rather than the single octopole present in our older configuration. The lengths of the first and second octopoles are 22.9 and 63.5 cm, respectively, and the distance between them is 1.0 mm. The rf voltage is the same for the two octopoles but the dc voltage on the second octopole is slightly more negative (by 0.3 V) for the current experiments. The first octopole passes through a gas cell of effective length 8.26 cm that contains the neutral collision partner, Xe here, at a fairly low pressure (0.05–0.2 mTorr). The unreacted parent and product ions drift to the end of the second octopole from which they are extracted, passed through a quadrupole mass filter for mass analysis, and detected with a secondary electron scintillation ion detector using standard pulse counting techniques. Raw ion intensities are converted to cross-sections as described previously [24]. Absolute

cross section magnitudes are estimated to be accurate to ±20%,whereas relative cross sections are accurate to ±5%.

Laboratory (lab) energies are converted to center-of-mass (CM) energies using the conversion $E_{CM} = E_{lab}M/(M + m)$, where M and m are the neutral and ion masses, respectively. All energies cited below are in the CM frame unless otherwise noted. The absolute energy scale and corresponding full width at half-maximum (FWHM) of the ion beam kinetic energy distribution are determined using the octopole as a retarding energy analyzer as described previously [24]. Because the reaction zone and the energy analysis region are physically the same, ambiguities in the energy analysis resulting from contact potentials, space charge effects, and focusing aberrations are minimized [24]. The energy distributions are nearly Gaussian and have typical FWHMs of 0.2–0.4 eV (lab).

It has been shown previously [29–31] that the shape of CID cross sections of ionic complexes is often affected by multiple collisions with the neutral reactant gas, even when the neutral gas pressure is fairly low. Because the presence and magnitude of these pressure effects is difficult to predict, we measured the pressure dependence of all cross sections examined here. Three xenon pressures were used, approximately 0.20, 0.10, and 0.05 mTorr, for all of the $L_1Na^+L_2$ systems. In the present systems, we found slight to marked dependence on the xenon pressure in the collision cell. All cross sections shown below and all threshold analyses reported here are for data that have been extrapolated to zero reactant pressure, as described previously [30], and therefore represent rigorously single collision conditions.

2.2. Ion source

The sodium cation complexes are formed in a 1 m long flow tube [25,30] operating at a pressure of 0.6–0.9 Torr with helium flow rates of 6 500–8 500 sccm. Sodium ions are generated in a continuous dc discharge by argon ion sputtering of a tantalum cathode with a cavity containing sodium metal. Typical operating conditions of the discharge source are 1.8–2.5 kV and 12–22 mA in a flow of roughly 10% argon in helium. Vapors of the ligands are introduced into the flow approximately 50 cm downstream from the dc discharge. The $L_1Na^+L_2$ complexes are formed by associative reactions of the sodium cations with the neutral ligands and are stabilized by collisions with the surrounding bath gas. The flow conditions used in this ion source provide greater than 10^4 collisions with the He buffer gas, such that the ions are believed to be thermalized to 300 K, both vibrationally and rotationally. In our analysis of the data, we assume that the ions are in their ground electronic states and that their internal energy is well characterized by a Maxwell–Boltzmann distribution of rovibrational states at 300 K. Previous work from this laboratory has shown that these assumptions are generally valid [29–35].

2.3. Thermochemical analysis

As described in detail previously [23], the threshold regions of the competitive collision-induced dissociation cross sections are modeled using

$$\sigma_m(E) = (n\sigma_{0,m}/E)\sum_i g_i \int_0^{E+E_1-E_{0,m}} \cdot [k_m(E^*)/k_{tot}(E^*)][1 - e^{-k_{tot}(E^*)\tau}](\Delta E)^{n-1} d(\Delta E) \quad (1)$$

where n is an adjustable parameter, $\sigma_{0,m}$ is an energy-independent scaling factor for channel m, E is the relative translational energy of the reactant ion and neutral, $E_{0,m}$ is the CID threshold at 0 K for channel m, τ is the experimental time for dissociation (~5×10^{-4} s in the extended dual octopole), ΔE is the energy that remains in translation after the collision between the reactants, and E^* is internal energy of the energized molecule (EM) after the collision, i.e. $E^* = E + E_i - \Delta E$. The term $k_m(E^*)$ is the unimolecular rate constant for dissociation to channel m. This rate constant and $k_{tot}(E^*)$ are defined using Rice-Ramsperger-Kassel-Marcus (RRKM) theory as [36–38],

$$k_{tot}(E^*) = \sum_m k_m(E^*) = \sum_m d_m N_m^\dagger(E^* - E_{0,m})/h\rho(E^*) \quad (2)$$

where d_m is the reaction degeneracy, $N_m^\dagger(E^*-E_{0,m})$ is the sum of rovibrational states of the transition state (TS) for channel m at an energy $E^*-E_{0,m}$, and $\rho(E^*)$ is the density of states of the EM at the available energy, E^*. The summation in Eq. (1) is over the rovibrational states of the reactant ion, i, where E_i and g_i are the energy and the population ($\Sigma g_i = 1$) of each state, respectively. The populations of rovibrational excited levels are not negligible at 300 K as a result of the many low-frequency modes present in these $L_1Na^+L_2$ complexes. The relative reactivities of all ro vibrational states, as reflected by the parameters $\sigma_{0,m}$ and n, are assumed to be equivalent. Vibrational frequencies and rotational constants for the $L_1Na^+L_2$ complexes are taken from ab initio calculations and scaled to bring the calculated frequencies into agreement with the experimentally determined frequencies as found by Pople and coworkers [39,40]. The Beyer–Swinehart algorithm [41–43] is used to evaluate the rovibrational density of states of the reactant ions and the relative populations, g_i, are calculated by a Maxwell–Boltzmann distribution at 300 K. The scaled vibrational frequencies for the reactants and all products were simultaneously increased and decreased by 10%, in order to estimate errors in the calculated frequencies. The uncertainty that this introduces into the analysis is included in the final uncertainties listed for the CID thresholds, $E_{0,m}$, and the other fitting parameters.

As mentioned above and described in detail elsewhere [32,33,44,45], statistical theories are used to determine the unimolecular rate constants for dissociation. This requires rovibrational frequencies for the energized molecules and the transition states (TSs) leading to dissociation. Because the metal–ligand interactions in the $L_1Na^+L_2$ complexes are largely electrostatic (ion-dipole, ion-induced dipole and ion-quadrupole interactions), the most appropriate model for the TS is a loose association of the ion and neutral ligand fragments. This TS is located at the centrifugal barrier for the interaction of L_1Na^+ with L_2 and L_2Na^+ with L_1. Therefore, the TS vibrations used here are the frequencies corresponding to the dissociation products. The previously calculated vibrational frequencies for $Na^+(C_2H_5OH)$, $Na^+(CH_3OH)$, $Na^+(C_6H_6)$, C_2H_5OH, CH_3OH, and C_6H_6 were used [3,19], whereas the vibrational frequencies for all other dissociation products were calculated as described below. The transitional modes, those that become rotations of the completely dissociated products, are treated as rotors, a treatment that corresponds to a phase space limit, described in detail elsewhere [44,45]. For the $L_1Na^+L_2$ complexes, there are five transitional modes for each of the two dissociation pathways, four of which are assigned as the 2-D rotors of the $L_1Na^+ + L_2$ and $L_2Na^+ + L_1$ products, with axes perpendicular to the reaction coordinate. Of the two rotations of the dissociation products with axes parallel to the reaction coordinate, one is the fifth transitional mode and the other becomes an external rotation of the TS. These rotations are taken to be the two 1D rotors of the $L_1Na^+ + L_2$ and $L_2Na^+ + L_1$ products. Assignment of which is the external rotor and which is the transitional mode is unnecessary as both modes are treated equivalently in the calculation of the kinetic rate constant. The 2D external rotational constant of the TS is determined variationally, as detailed elsewhere [44,45], and is treated adiabatically but with centrifugal effects included, consistent with the discussion of Waage and Rabinovitch [46]. The rotational constants of the energized molecule and the transition state for each $L_1Na^+L_2$ complex are available from the authors upon request.

The basic form of Eq. (1) is expected to be appropriate for translationally driven reactions [47] and has been found to reproduce reaction cross sections well for a number of previous studies of both atom-diatom and polyatomic reactions [48], including CID processes [3,16,17,20,31–35,44,49–53]. The model of Eq. (1) is convoluted with the kinetic energy distribution of the reactants and the parameters $\sigma_{0,m}$, n, and $E_{0,m}$ are optimized by performing a nonlinear least-squares analysis of the data. An estimate of the error associated with the measurement of $E_{0,m}$ is determined from the range of threshold values obtained for different data sets, for variation of the parameter n, for variations associated with the $\pm 10\%$ uncertainties in the vibrational frequencies, for the effects of increasing and decreasing the time available for the ions to dissociate (5×10^{-4} s) by factors of 2,

and for the error in the absolute energy scale, ±0.05 eV (lab).

Because all sources of internal energy are included in the data analysis of Eq. (1), the thresholds obtained correspond to the minimum energy necessary for dissociation, in other words, the 0 K value. This assumption has been tested for several systems [31–35,51]. It has been shown that treating all of the energy of the ion (vibrational, rotational, and translational) as capable of coupling with the reaction coordinate leads to reasonable thermochemistry. The 0 K threshold energies for the CID reactions of $L_1Na^+L_2$ with Xe, $E_{0,m}$, are converted to 0 K BDEs, $D_{0,m}$, by assuming that $E_{0,m}$ represents the energy difference between reactants and products at 0 K (for example, see Figure 1 [54]). This assumption requires that there are no activation barriers in excess of the bond endothermicities, which is generally true for ion-molecule reactions [48] and should be true for the simple heterolytic bond fission reactions examined here [55].

2.4. Computational details

Ab initio calculations were performed using GAUSSIAN 98 [56] for the $L_1Na^+L_2$ complex ions in order to obtain geometrical structures, vibrational frequencies, rotational constants, and the energetics of dissociation of the ions. Geometry optimizations were performed first at the RHF/6-31G* level, followed by optimization at the MP2(full)/6-31G* level. It was recently demonstrated that the MP2(full)/6-31G* level provides a reasonably good geometrical description of sodium cation complexes with various ligands, Na^+L [1–3]. Vibrational frequencies and rotational constants were determined at the MP2(full)/6-31G* level for the MP2(full)/6-31G* optimized structures of the $L_1Na^+L_2$ complexes. The lowest frequency for the $L_1Na^+L_2$ complexes was calculated to be a very low positive or negative value (-22–+31 cm^{-1}) and corresponds to the synchronous torsional motion of the two ligands about the L_1–Na^+–L_2 bond axis. For all $L_1Na^+L_2$ complexes, our data analysis treated this motion as a one-dimensional internal rotor, $I_{torsion} = I_1I_2/(I_1 + I_2)$, as described by Gilbert and Smith [36]. Because this motion is treated as an internal rotor, the reaction degeneracy needs to be adjusted to account for the additional rotational symmetry number associated with the torsional motion. This amounts to inclusion of a factor equal to the highest-fold rotational symmetry number of the two ligands about the L_1–Na^+–L_2 bond axis, e.g. for $(H_2O)Na^+(C_6H_6)$, this is a factor of 6. The vibrational frequencies and rotational constants, including the torsional motion, of the $L_1Na^+L_2$ species are available from the authors upon request. When used to model data or calculate thermal energy corrections, the MP2(full)/6-31G* calculated vibrational frequencies were scaled by a factor of 0.9646 [57].

In order to determine the L_1Na^+–L_2 bond energetics, single point energy calculations were performed at the MP2(full)/6-311+G(2d,2p) level using the MP2(full)/6-31G* optimized geometries of the $L_1Na^+L_2$ complexes. Using these energies and the energies of the sodium ion and the two neutral ligands, calculated at the same level, the bond energy sum for complete dissociation, i.e. Na^+–L_1L_2, was calculated. Basis set superposition errors (BSSE) in the calculated Na^+–L_1L_2 binding energies were estimated using the full counterpoise correction method [58,59]. The BSSE corrections ranged from 19.8 kJ/mol for $(C_6H_6)Na^+(C_2H_5OH)$ to 11.2 kJ/mol for $(H_2O)Na^+(NH_3)$. The calculated Na^+–L_1L_2 BDEs were also corrected for zero-point energies (ZPEs) using the scaled vibrational frequencies calculated at the MP2(full)/6-31G* level. The BSSE and ZPE corrected Na^+–L_1L_2 BDEs were then combined with the previous theoretical Na^+–L BDEs calculated at the same level of theory and corrected for ZPE and BSSE [3] to afford the desired L_1Na^+–L_2 BDEs.

3. Results

3.1. Collision-induced dissociation of $L_1Na^+L_2$

Collision-induced dissociation cross sections were obtained for fourteen doubly ligated complexes of the sodium cation, $L_1Na^+L_2$ (L_1, L_2= H_2O, C_6H_6, CH_3OH, CH_3OCH_3, NH_3 and C_2H_5OH), reacting

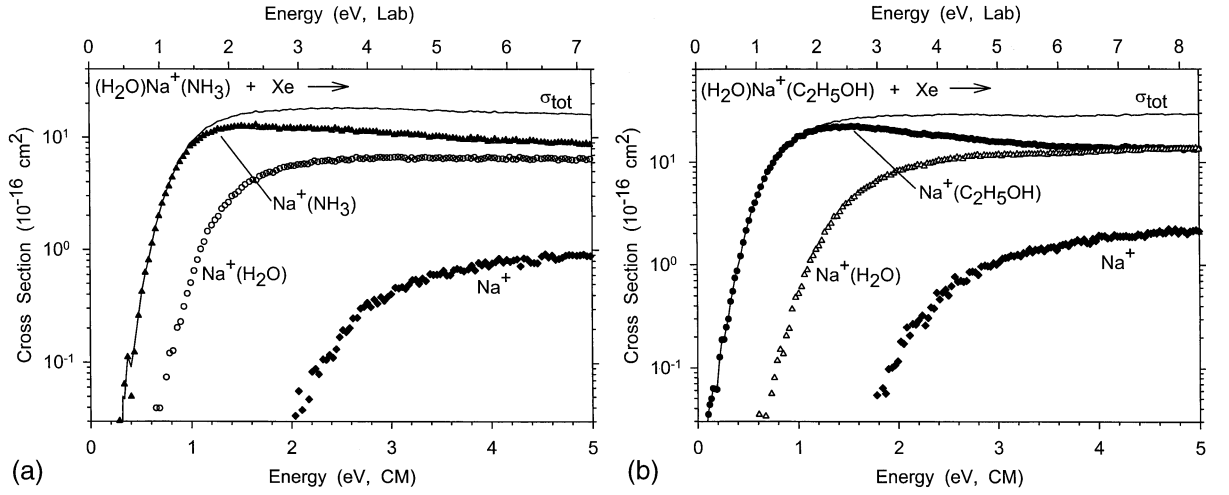

Fig. 1. Cross sections for collision-induced dissociation of (a) $(H_2O)Na^+(NH_3)$ and (b) $(H_2O)Na^+(C_2H_5OH)$ with xenon as a function of kinetic energy in the center-of-mass frame (lower axis) and laboratory frame (upper axis). Solid lines show the total cross section for each system and the symbols represent data extrapolated to zero pressure.

with xenon. No systems where $L_1 = L_2$ were studied here (although those for H_2O, C_6H_6, and CH_3OCH_3 have been studied previously [16,17,20]) and the $(CH_3OCH_3)Na^+(C_2H_5OH)$ complex cannot be studied because these ligands have the same mass. Representative CID data are shown in Fig. 1 for $(H_2O)Na^+(NH_3)$ and $(H_2O)Na^+(C_2H_5OH)$ complexes and Fig. 2 for $(H_2O)Na^+(C_6H_6)$, and $(NH_3)Na^+(C_2H_5OH)$ complexes. A complete set of figures for the CID data of the ten remaining $L_1Na^+L_2$ systems examined can be obtained from the authors upon request. In two systems, $L_1 = H_2O$ and $L_2 = C_6H_6$ or CH_3OH, we also used argon as the collision gas. The $(H_2O)Na^+(C_6H_6)$ complex was one of the more difficult systems to model, so the alternative set of data was obtained to check whether using a more

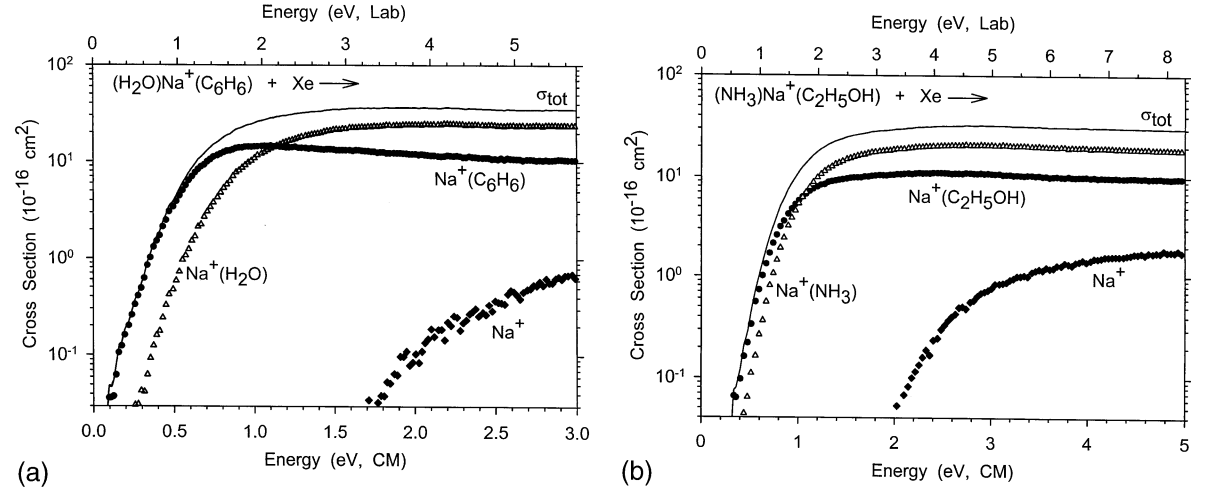

Fig. 2. Cross sections for collision-induced dissociation of (a) $(H_2O)Na^+(C_6H_6)$ and (b) $(NH_3)Na^+(C_2H_5OH)$ with xenon as a function of kinetic energy in the center-of-mass frame (lower axis) and laboratory frame (upper axis). Solid lines show the total cross section for each system and the symbols represent data extrapolated to zero pressure.

favorable laboratory to center-of-mass conversion might provide a different shape to the cross sections. We found that the Ar and Xe data yield virtually identical cross sections for both systems and modeling of the data yields the same thresholds within the cited experimental errors.

The dominant processes observed for all systems are the losses of the intact ligands, reaction 3, over the energy ranges examined, 0 to 3–6 eV.

$$L_1Na^+L_2 + Xe \rightarrow L_1Na^+ + L_2 + Xe \quad (3a)$$

$$\rightarrow L_2Na^+ + L_1 + Xe \quad (3b)$$

The CID cross sections for $(H_2O)Na^+(NH_3)$ and $(H_2O)Na^+(C_2H_5OH)$, Figs. 1(a) and (b), are typical results observed in our laboratory for competitive dissociation of doubly ligated metal ion complexes [23]. In these systems, the cross section for the formation of the lowest energy process rises rapidly from baseline with increasing energy. The cross section then begins to level off and declines at higher energies. The formation of the higher energy Na^+L product has a cross section that rises more slowly than the lower energy channel, but its increase corresponds with the leveling off and decline of the first product channel. This behavior indicates that the two dissociation channels are indeed in competition with one another. Another sign of this competition is the smooth increase in the total cross section as energy is varied. At the highest energies examined, the sequential loss of both ligands can occur, forming Na^+.

All other complexes examined in this work behave similarly to the examples shown in Figs. 1(a) and 1(b), except for two. The CID data for $(H_2O)Na^+(C_6H_6)$ and $(C_2H_5OH)Na^+(NH_3)$, Figs. 2(a) and 2(b), respectively, are less typical of results obtained for bis-ligated metal complexes [23,60]. They involve complexes where the relative binding energies of the two ligands differ by less than 0.1 eV, but are not unique in this regard. Again, the lowest energy process has a Na^+L cross-section that rises rapidly with increasing energy. The cleavage of the other Na^+L bond begins to occur at a slightly higher energy, but the cross section for the formation of this ion becomes the more probable process at higher energies, such that the two cross sections cross one another. This type of crossing was observed for the $(2\text{-}C_3H_7OH)Li^+(1\text{-}C_4H_9OH)$ complex in our previous competitive CID study [23]. The implications of such results in regards to the use of the kinetic method [61–63] have been discussed previously [64]. The current observations of systems behaving this way further illustrate the possibility of arriving at erroneous conclusions by use of the simple kinetic method (that where entropic effects are presumed to cancel). It is more difficult to speculate about the implications for the extended kinetic method, which includes the possibility of differing entropies of dissociation; however, the extended kinetic method presumes that these entropies are similar for all reference compounds. As will be seen below, this is definitely not the case for ethanol vs. the other ligands considered here. Overall, such results clearly demonstrate the need for examining the energy dependence of competitive dissociation to provide accurate thermodynamic information.

3.2. Thermochemical results

3.2.1. Competitive threshold analysis

In our previous competitive CID study using guided ion beam mass spectrometry [23], we showed that the best measure of the dissociation thresholds, $E_{0,m}$, for metal–ligand complex ions in which competition occurs comes from the simultaneous analysis of the cross sections for these dissociation products, reactions 3 in the current $L_1Na^+L_2$ systems. These competitive CID processes were analyzed using Eq. (1) with explicit integration over the rotational energy distribution, as described previously [45, 65]. It is also worth noting that we did analyze the data using the average rotational energy in the rate constant calculation rather than an explicit integration over the rotational distribution. As concluded previously [3], this approach leads to results that are in poorer agreement with the literature values than those determined with the integration method, both in terms of relative order and with respect to quantitative agreement. The details of these alternate evaluations are not presented in this work. Ideally, the two cross sections

should be modeled using a single scaling factor, $\sigma_{o,m}$, for the two channels such that the energy dependent ratio of the cross section magnitudes is determined solely by the statistical rate constant ratio, $k_m(E^*)/k_{tot}(E^*)$. However, in our previous competitive CID study of lithium ions complexed with alcohols and water [23], it was found that the use of a single scaling factor caused difficulties in some systems with reproducing the data for both channels over a fairly extended energy range. Therefore, the ability to model each channel with an independent scaling factor, $\sigma_{o,m}$, was introduced into the analysis. This added flexibility did not change the final relative and absolute bond energies for the Li^+ complexes significantly, as compared to when a single scaling factor was used, and therefore the results reported for that study were those determined with independent scaling factors. In the present work, the data for all systems was analyzed both with independent and common scaling factors because differences in the relative and absolute bond energies were observed between the two methods. The results of these analyses are presented in Tables 1 and 2, respectively.

For four of the systems examined, $(H_2O)Na^+(NH_3)$, $(C_6H_6)Na^+(NH_3)$, $(C_6H_6)Na^+(CH_3OH)$, and $(C_6H_6)Na^+(CH_3OCH_3)$, comparable fits were obtained over the same energy ranges using both independent and common scaling factors. This is shown for $(H_2O)Na^+(NH_3)$ in Figs. 3(a) and 3(b). In both cases, the models reproduce the data very well for each channel up to energy of approximately 1.6 eV. For the other ten systems, however, this was not the case. An example of these systems is $(CH_3OH)Na^+(CH_3OCH_3)$, as shown in Figs. 4(a)–4(c). A complete set of figures for all systems showing the analysis using independent and common scaling factors can be obtained from the authors upon request. As can be seen in Fig. 4(a), the quality of the fit to the data using independent scaling factors is quite good up to an energy of approximately 1.7 eV for both channels. If a common scaling factor is then used and the fitting parameters in Eq. (1) are optimized over the same 1.7 eV energy range, the fits shown in Fig. 4(b) result. For both channels, the model does not reproduce the data particularly well. However, good reproduction of the data in the threshold region can be obtained over a smaller energy range (up to 1.2 eV in the present case), as displayed in Fig. 4(c). We believe that the smaller energy range for the common scaling factor analysis is reasonable because the threshold region is the most important portion of the data to reproduce accurately.

Among the various systems for which a common scaling factor reproduced the data poorly was $(NH_3)Na^+(C_2H_5OH)$. As shown in Fig. 5(a), reproduction of the data with independent scaling factors is excellent over an extended energy range and the crossing between the two channels is accurately modeled. When a common scaling factor is used, however, the models for each channel no longer cross and the data are reproduced only up to about 0.8 eV, Fig 5(b). In considering why our statistical analysis of this system failed so badly, we noted that the ethanol ligand has two internal rotors that are tied up in the reactant $(NH_3)Na^+(C_2H_5OH)$ and product $Na^+(C_2H_5OH)$ complexes because both the hydroxy and methyl ends of the molecule complex to the metal ion (see computational results below). Hence, we tried modeling the data treating the two internal rotors as free rotors (including a symmetry number of three for the methyl rotor) [66] but only in the $Na^+(NH_3) + C_2H_5OH$ product channel. This dramatically improved the ability to reproduce the data over a much wider energy range using common scaling factors. We then considered whether the internal rotors of the ethanol product should be treated as a hindered rotor, i.e. as a vibration at low energies and as a free rotor at high energies (including a symmetry number of three for the methyl rotor). To do this, we use the treatment of hindered rotors outlined by DeTuri and Ervin [65] (which is presently implemented in our data analysis program, CRUNCH). When both the methyl and hydroxy rotors are treated as hindered, the model with a common scaling factor is shown in Fig. 5(c). This can be seen to reproduce the data well over a broad energy range. Indeed, reproduction of the data treating the internal modes as rotors (hindered or free) is essentially equivalent. However, there are small differences in the thresholds obtained using these various treatments and these are shown in Table 3. It can be seen that changing the internal rotors from vibrations

Table 1
Competitive fitting parameters of Eq. (1) with independent scaling factors, threshold dissociation energies at 0 K, and entropies of activation at 1000 K

Complex	Ionic Product	Rxn Deg[a]	σ_0	n	E_0 (eV)	ΔE_0 (eV)	$\Delta S^{\dagger}$ (J/K mol)
$(H_2O)Na^+(C_6H_6)$	$Na^+(C_6H_6)$	1.0	33 (8)	0.6 (0.1)	0.78 (0.05)	0.158 (0.013)	3 (4)
	$Na^+(H_2O)$	0.5	138 (34)		0.94 (0.05)		32 (4)
$(H_2O)Na^+(CH_3OH)$	$Na^+(CH_3OH)$	1.0	33 (2)	0.6 (0.1)	0.88 (0.05)	0.149 (0.013)	11 (4)
	$Na^+(H_2O)$	1.0	112 (15)		1.03 (0.05)		16 (4)
$(H_2O)Na^+(NH_3)$	$Na^+(NH_3)$	0.5	30 (2)	0.8 (0.1)	0.85 (0.05)	0.136 (0.025)	4 (4)
	$Na^+(H_2O)$	0.5	36 (8)		0.99 (0.06)		14 (4)
$(H_2O)Na^+(CH_3OCH_3)$	$Na^+(CH_3OCH_3)$	1.0	44 (2)	0.8 (0.1)	0.81 (0.05)	0.212 (0.010)	13 (4)
	$Na^+(H_2O)$	1.0	324 (43)		1.02 (0.05)		20 (4)
$(H_2O)Na^+(C_2H_5OH)$	$Na^+(C_2H_5OH)$	1.0	42 (2)	0.8 (0.1)	0.80 (0.05)	0.257 (0.015)	10(4)
	$Na^+(H_2O)$	1.0	296 (79)		1.06 (0.05)		22 (4)
$(H_2O)Na^+(C_2H_5OH)$[b]	$Na^+(C_2H_5OH)$	1.0	44 (2)	0.9 (0.1)	0.79 (0.05)	0.251 (0.015)	10 (4)
	$Na^+(H_2O)$	0.33	72 (16)		1.04 (0.05)		33 (4)[c]
$(C_6H_6)Na^+(CH_3OH)$	$Na^+(CH_3OH)$	0.5	76 (4)	1.0 (0.1)	0.84 (0.05)	0.039 (0.011)	30 (4)
	$Na^+(C_6H_6)$	1.0	109 (26)		0.88 (0.05)		6 (4)
$(C_6H_6)Na^+(CH_3OCH_3)$	$Na^+(CH_3OCH_3)$	0.5	106 (8)	1.2 (0.1)	0.82 (0.05)	0.068 (0.010)	30 (4)
	$Na^+(C_6H_6)$	1.0	177 (32)		0.89 (0.05)		9 (4)
$(C_6H_6)Na^+(NH_3)$	$Na^+(NH_3)$	0.5	83 (8)	1.0 (0.1)	0.84 (0.05)	0.061 (0.025)	39 (4)
	$Na^+(C_6H_6)$	1.0	46 (26)		0.90 (0.06)		20 (4)
$(C_6H_6)Na^+(C_2H_5OH)$	$Na^+(C_2H_5OH)$	0.5	86 (3)	0.9 (0.1)	0.84 (0.05)	0.169 (0.019)	32 (4)
	$Na^+(C_6H_6)$	1.0	391 (204)		1.01 (0.05)		15 (4)
$(C_6H_6)Na^+(C_2H_5OH)$[b]	$Na^+(C_2H_5OH)$	0.5	87 (3)	0.9 (0.1)	0.85 (0.05)	0.154 (0.019)	32 (4)
	$Na^+(C_6H_6)$	0.33	85 (12)		1.00 (0.05)		26 (4)[c]
$(CH_3OH)Na^+(CH_3OCH_3)$	$Na^+(CH_3OCH_3)$	1.0	54 (3)	0.8 (0.1)	0.91 (0.06)	0.059 (0.008)	9 (4)
	$Na^+(CH_3OH)$	1.0	110 (9)		0.97 (0.06)		11 (4)
$(CH_3OH)Na^+(NH_3)$	$Na^+(NH_3)$	1.0	61 (4)	1.1 (0.1)	0.97 (0.06)	0.024 (0.010)	13 (4)
	$Na^+(CH_3OH)$	1.0	26 (3)		0.99 (0.06)		17 (4)
$(CH_3OH)Na^+(C_2H_5OH)$	$Na^+(C_2H_5OH)$	1.0	57 (3)	0.8 (0.1)	0.92 (0.05)	0.120 (0.014)	9 (4)
	$Na^+(CH_3OH)$	1.0	114 (24)		1.04 (0.05)		16 (4)
$(CH_3OH)Na^+(C_2H_5OH)$[b]	$Na^+(C_2H_5OH)$	1.0	69 (3)	1.0 (0.1)	0.90 (0.0.05)	0.126 (0.014)	9 (4)
	$Na^+(CH_3OH)$	0.33	50 (11)		1.03 (0.05)		28 (4)[c]
$(CH_3OCH_3)Na^+(NH_3)$	$Na^+(CH_3OCH_3)$	0.5	24 (2)	1.1 (0.1)	0.98 (0.06)	0.014 (0.006)	13 (4)
	$Na^+(NH_3)$	0.5	99 (3)		0.99 (0.06)		11 (4)
$(NH_3)Na^+(C_2H_5OH)$	$Na^+(C_2H_5OH)$	1.0	23 (1)	0.8 (0.1)	0.92 (0.05)	0.119 (0.006)	18 (4)
	$Na^+(NH_3)$	1.0	220 (9)		1.04 (0.05)		21 (4)
$(NH_3)Na^+(C_2H_5OH)$[b]	$Na^+(C_2H_5OH)$	1.0	48 (2)	0.9 (0.1)	0.98 (0.05)	0.071 (0.006)	18 (4)
	$Na^+(NH_3)$	0.33	58 (2)		1.05 (0.05)		32 (4)[c]

[a] Reaction degeneracy: defined as the ratio of rotational symmetry numbers (including internal rotors) of the reactant to the products in the PSL TS.

[b] Values obtained by treating the ethanol internal rotors in the $Na^+(NH_3) + C_2H_5OH$ channel as hindered methyl and hydroxy rotors.

[c] $\Delta S^{\dagger}$ value obtained by treating the ethanol rotors in the $Na^+(NH_3) + C_2H_5OH$ channel as free methyl and hydroxy rotors.

to a hindered rotor increases the difference in thresholds between the two channels and changing to a free rotor increases the difference further. Note that treating both rotors as hindered yields a threshold difference somewhat less than the value cited for a hindered methyl rotor and free OH rotor, but not as low as the value obtained using two vibrations.

Of course, the treatment of the internal rotors of ethanol should not be confined to the $(NH_3)Na^+(C_2H_5OH)$ complex. If we analyze all four complexes containing ethanol and treat the internal rotors of the free ethanol product either as free or hindered rotors, we obtain the thresholds given in Table 3. In all four cases, this treatment allowed the data to be reproduced much more accurately over a wider energy range when a common scaling factor

Table 2
Competitive fitting parameters of Eq. (1) with common scaling factors, threshold dissociation energies at 0 K, and entropies of activation at 1000 K

Complex	Ionic Product	Rxn Deg[a]	σ_0	n	E_0(eV)	ΔE_0(eV)	$\Delta S^{\dagger}$ (J/K mol)
$(H_2O)Na^+(C_6H_6)$	$Na^+(C_6H_6)$	1.0	51 (16)	0.8 (0.3)	0.79 (0.06)	0.110 (0.008)	3 (4)
	$Na^+(H_2O)$	0.5			0.90 (0.06)		33 (4)
$(H_2O)Na^+(CH_3OH)$	$Na^+(CH_3OH)$	1.0	42 (9)	0.8 (0.2)	0.86 (0.06)	0.110 (0.010)	11 (4)
	$Na^+(H_2O)$	1.0			0.97 (0.06)		16 (4)
$(H_2O)Na^+(NH_3)$	$Na^+(NH_3)$	0.5	32 (2)	0.9 (0.1)	0.86 (0.05)	0.127 (0.006)	4 (4)
	$Na^+(H_2O)$	0.5			0.99 (0.05)		14 (4)
$(H_2O)Na^+(CH_3OCH_3)$	$Na^+(CH_3OCH_3)$	1.0	54 (5)	1.1 (0.2)	0.78 (0.05)	0.147 (0.011)	13 (4)
	$Na^+(H_2O)$	1.0			0.93 (0.05)		21 (4)
$(H_2O)Na^+(C_2H_5OH)$	$Na^+(C_2H_5OH)$	1.0	49 (7)	1.1 (0.3)	0.76 (0.07)	0.189 (0.014)	10 (4)
	$Na^+(H_2O)$	1.0			0.95 (0.07)		23 (4)
$(H_2O)Na^+(C_2H_5OH)^b$	$Na^+(C_2H_5OH)$	1.0	47 (7)	1.0 (0.2)	0.80 (0.07)	0.228 (0.014)	10 (4)
	$Na^+(H_2O)$	0.33			1.03 (0.07)		34 (4)[c]
$(C_6H_6)Na^+(CH_3OH)$	$Na^+(CH_3OH)$	0.5	79 (6)	1.0 (0.1)	0.84 (0.05)	0.030 (0.007)	30 (4)
	$Na^+(C_6H_6)$	1.0			0.87 (0.05)		6 (4)
$(C_6H_6)Na^+(CH_3OCH_3)$	$Na^+(CH_3OCH_3)$	0.5	108 (8)	1.2 (0.1)	0.82 (0.05)	0.054 (0.007)	30 (4)
	$Na^+(C_6H_6)$	1.0			0.87 (0.05)		9 (4)
$(C_6H_6)Na^+(NH_3)$	$Na^+(NH_3)$	0.5	80 (6)	1.0 (0.1)	0.84 (0.05)	0.087 (0.009)	39 (4)
	$Na^+(C_6H_6)$	1.0			0.93 (0.05)		19 (4)
$(C_6H_6)Na^+(C_2H_5OH)$	$Na^+(C_2H_5OH)$	0.5	88 (3)	0.9 (0.1)	0.85 (0.05)	0.107 (0.010)	32 (4)
	$Na^+(C_6H_6)$	1.0			0.96 (0.05)		16 (4)
$(C_6H_6)Na^+(C_2H_5OH)^b$	$Na^+(C_2H_5OH)$	0.5	88 (3)	0.9 (0.1)	0.85 (0.05)	0.155 (0.010)	32 (4)
	$Na^+(C_6H_6)$	0.33			1.00 (0.05)		27 (4)[c]
$(CH_3OH)Na^+(CH_3OCH_3)$	$Na^+(CH_3OCH_3)$	1.0	72 (5)	1.0 (0.1)	0.89 (0.06)	0.037 (0.006)	9 (4)
	$Na^+(CH_3OH)$	1.0			0.93 (0.06)		12 (4)
$(CH_3OH)Na^+(NH_3)$	$Na^+(NH_3)$	1.0	53 (8)	1.3 (0.3)	0.93 (0.07)	0.064 (0.013)	13 (4)
	$Na^+(CH_3OH)$	1.0			0.99 (0.07)		17 (4)
$(CH_3OH)Na^+(C_2H_5OH)$	$Na^+(C_2H_5OH)$	1.0	86 (14)	1.4 (0.3)	0.85 (0.07)	0.099 (0.004)	9 (4)
	$Na^+(CH_3OH)$	1.0			0.95 (0.07)		16 (4)
$(CH_3OH)Na^+(C_2H_5OH)^b$	$Na^+(C_2H_5OH)$	1.0	68 (14)	1.0 (0.2)	0.89 (0.07)	0.139 (0.007)	9 (4)
	$Na^+(CH_3OH)$	0.33			1.03 (0.07)		28 (4)[c]
$(CH_3OCH_3)Na^+(NH_3)$	$Na^+(NH_3)$	0.5	76 (11)	1.6 (0.3)	0.90 (0.06)	0.034 (0.010)	12 (4)
	$Na^+(CH_3OCH_3)$	0.5			0.93 (0.06)		13 (4)
$(NH_3)Na^+(C_2H_5OH)$	$Na^+(C_2H_5OH)$	1.0	48 (6)	1.0 (0.2)	0.95 (0.06)	0.047 (0.010)	18 (4)
	$Na^+(NH_3)$	1.0			1.00 (0.06)		21 (4)
$(NH_3)Na^+(C_2H_5OH)^b$	$Na^+(C_2H_5OH)$	1.0	56 (6)	1.1 (0.2)	0.95 (0.06)	0.063 (0.010)	18 (4)
	$Na^+(NH_3)$	0.33			1.01 (0.06)		32 (4)[c]

[a] Reaction degeneracy: defined as the ratio of rotational symmetry numbers (including internal rotors) of the reactant to the products in the PSL TS.

[b] Values obtained treating the ethanol internal rotors in the $Na^+(NH_3) + C_2H_5OH$ channel as hindered methyl and hydroxy rotors.

[c] $\Delta S^{\dagger}$ value obtained by treating the ethanol rotors in the $Na^+(NH_3) + C_2H_5OH$ channel as free methyl and hydroxy rotors.

was used. Complete sets of fitting parameters using common scaling for the case where both the methyl and hydroxy rotors are hindered are included in Table 2. Table 1 includes comparable parameters where independent scaling factors are used. Comparison of the $\sigma_{0,m}$ values in Table 1 shows that large differences in the relative scaling factors have been reduced or eliminated in all four cases, an indication that the independent scaling factors were accommodating the failure to properly treat these internal modes.

At this point, it is relevant to ask whether other ligands should also have internal rotors that must be considered similarly. Clearly, H_2O, NH_3, and C_6H_6 do not, but methanol and dimethyl ether might. Note however that in complexes of these ligands the internal rotors are not eliminated by complexation as

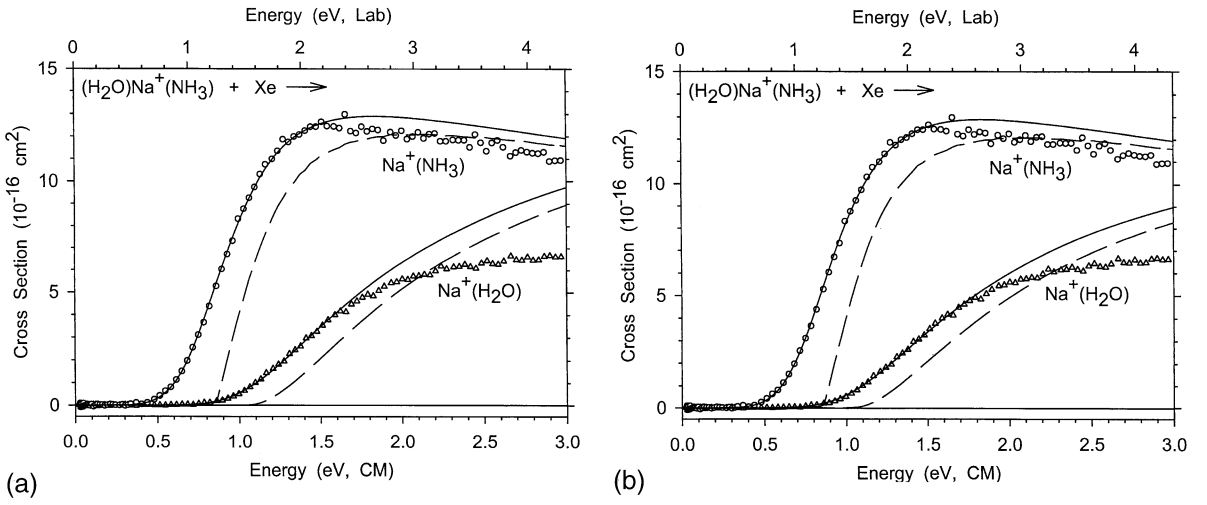

Fig. 3. Zero pressure extrapolated cross sections for the competitive collision-induced dissociation processes of $(H_2O)Na^+(NH_3)$ with xenon in the threshold region as a function of kinetic energy in the center-of-mass frame (lower axis) and laboratory frame (upper axis). Solid lines show the best fits to the data using the model of Eq. (1) convoluted over the neutral and ion kinetic energies and the internal energies of the reactants, using (a) independent and (b) common scaling factors. Dashed lines show the model cross-sections in the absence of experimental energy broadening for reactants with an internal energy of 0 K.

they are in the case of ethanol. As a test case, we treated the two methyl rotors of dimethyl ether as free or hindered rotors in the reactant and product complexes and the product ligand. We observed no significant change in the fitting parameters from those obtained treating these internal rotors as vibrations. Therefore it is the difference in the complexed ethanol ligand (where there are no internal rotors of the ligand) vs. the free ligand (where there are two internal rotors) that leads to the large changes in the modeling observed here.

3.2.2 Relative and absolute Na^+–L bond dissociation energies

Measurement of the threshold energies for the dissociation processes (3) provide absolute metal–ligand bond energies for the second ligand. However, it has been pointed out previously [23] that relative bond energies for the first ligands can be obtained from the relative thresholds measured for competitive CID of doubly ligated metal ion complexes, $\Delta E_0 = D[L_2M^+–L_1] – D[L_1M^+–L_2]$. Because the sum of the two bond energies is independent of the order in which the ligands are removed, ΔE_0 also equals the relative binding energy of the metal ion to the two individual ligands, $D[M^+–L_1] – D[M^+–L_2]$. The relative thresholds, ΔE_0, determined here are given in Tables 1 and 2. The relative M^+–L bond energies can then be converted to absolute M^+–L bond energies using a reliable absolute metal–ligand bond energy as an anchor value. The advantage of using competitive CID of doubly ligated metal ion complexes to determine the absolute BDEs of singly ligated metal ion complexes is that the relative thresholds measured using this method are more precise than those determined from independent absolute CID measurements [23]. Such measurements are particularly useful in resolving discrepancies in the literature or for relative binding energies that are smaller than the uncertainties obtained in the absolute CID measurements (typically ± 0.05–0.10 eV). For the present work, we have chosen to use the absolute Na^+–NH_3 bond dissociation energy, 102.2 ± 5.4 kJ/mol, previously determined in our laboratory [3] as the anchor value. This is because the absolute BDE for this system determined by CID was found to be in best agreement with previous literature experimental values [1,2] and theoretical values at

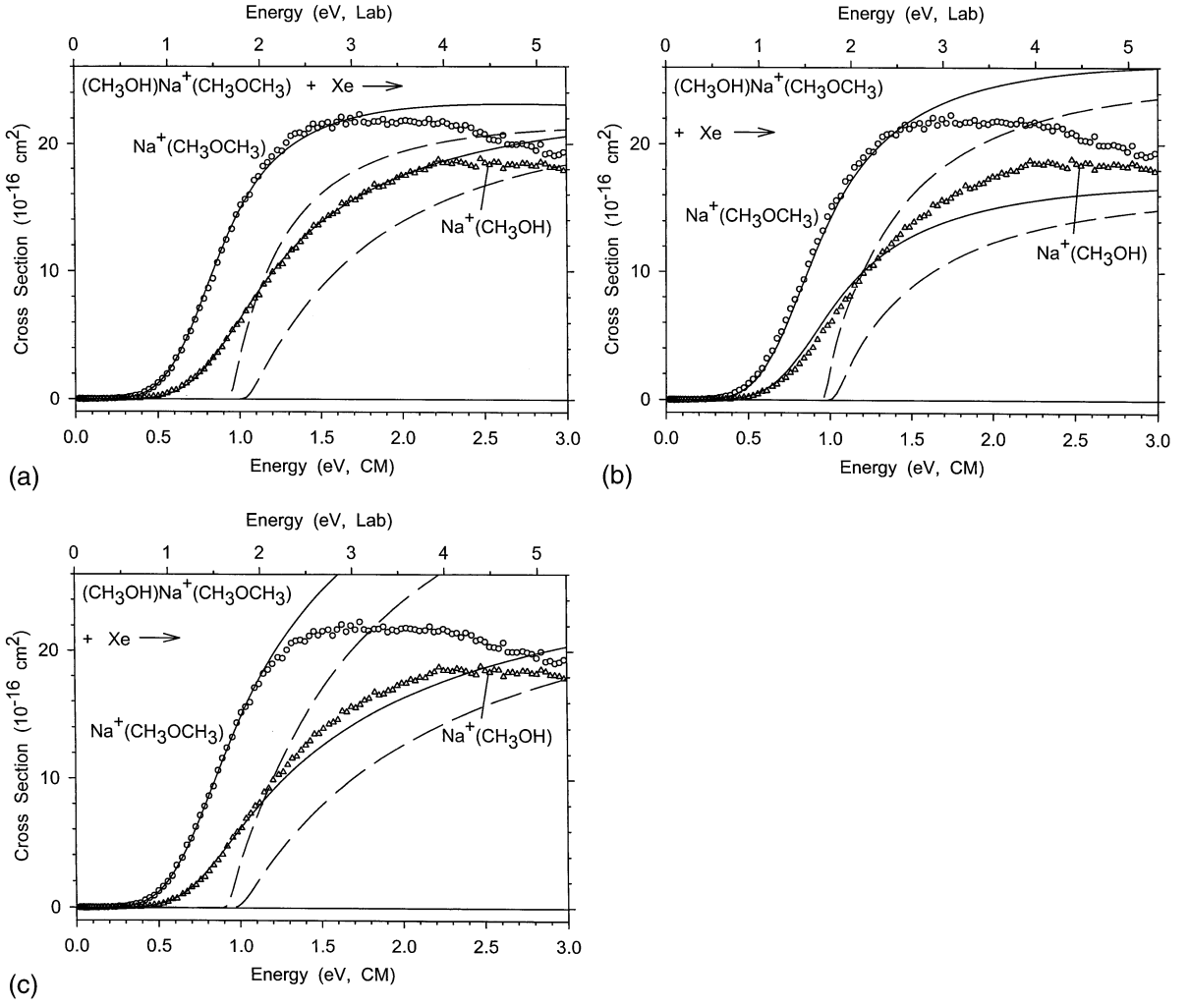

Fig. 4. Zero pressure extrapolated cross sections for the competitive collision-induced dissociation processes of $(CH_3OH)Na^+(CH_3OCH_3)$ with xenon in the threshold region as a function of kinetic energy in the center-of-mass frame (lower axis) and laboratory frame (upper axis). Solid lines show the best fits to the data using the model of Eq. (1) convoluted over the neutral and ion kinetic energies and the internal energies of the reactants, using (a) independent and (b) and (c) common scaling factors. Dashed lines show the model cross-sections in the absence of experimental energy broadening for reactants with an internal energy of 0 K. In part (b), the fitting parameters are optimized over the same energy range as that shown for part (a), 0.0–1.7 eV, whereas in part (c), the fitting parameters are optimized over a smaller energy range, 0.0–1.2 eV.

several levels of theory [3]. This choice will be further evaluated below.

To determine the best set of relative sodium ion binding affinities, we use a least squares minimization of the deviations of the relative values from the experimental relative thresholds (χ^2) using the procedure detailed by DeTuri and Ervin [65]. These relative values are referenced arbitrarily to NH_3 as zero. We considered several sets of experimental values, Table 4, including both independent and common scaling procedures with two treatments of the internal rotors of the ethanol product: treated as (a) vibrations and (b) hindered methyl and hydroxy rotors. To determine absolute Na^+–L BDEs, these relative sodium ion binding affinities are combined with the absolute anchor value for Na^+–NH_3.

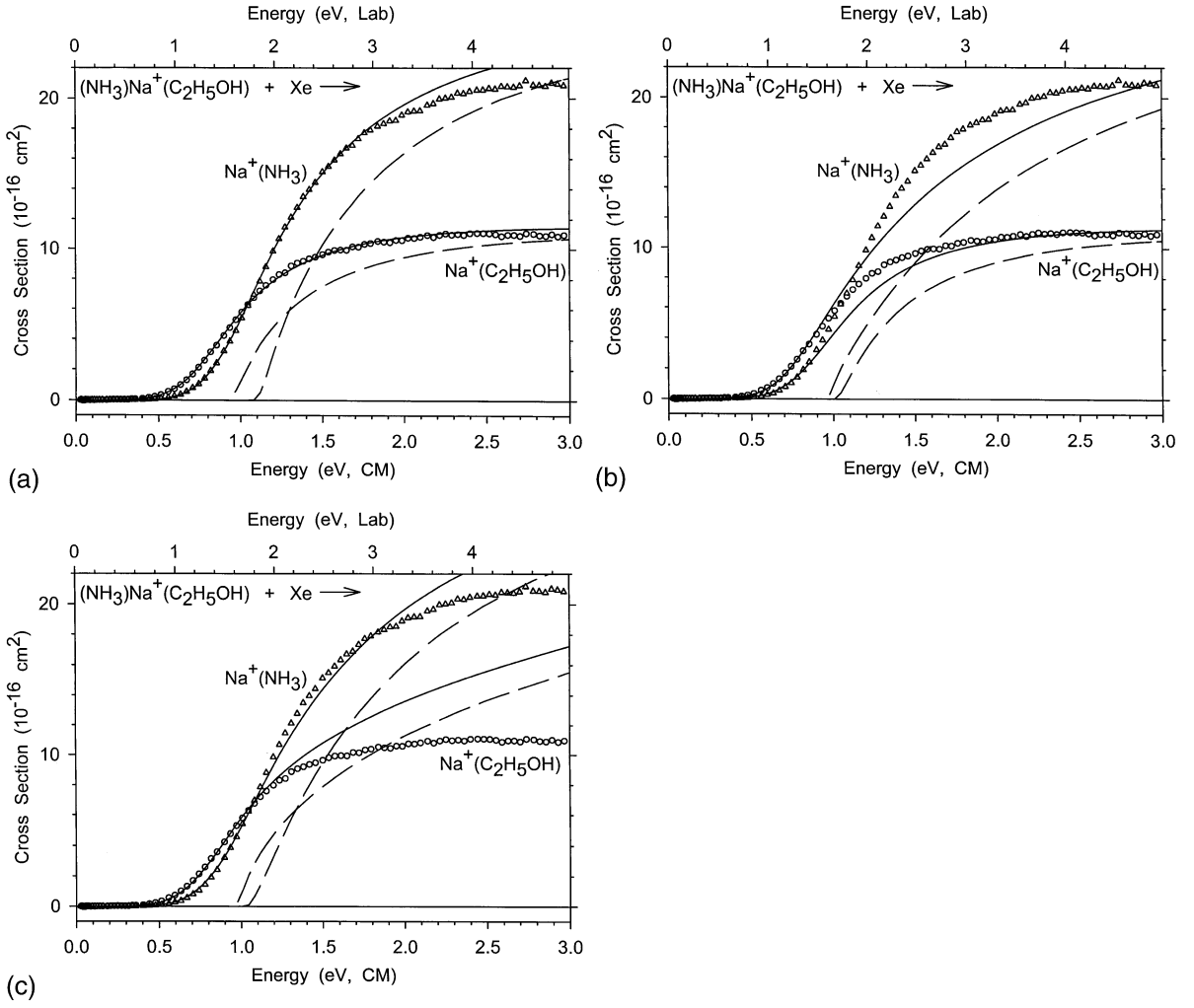

Fig. 5. Zero pressure extrapolated cross sections for the competitive collision-induced dissociation processes of $(NH_3)Na^+(C_2H_5OH)$ with xenon in the threshold region as a function of kinetic energy in the center-of-mass frame (lower axis) and laboratory frame (upper axis). Solid lines show the best fits to the data using the model of Eq. (1) convoluted over the neutral and ion kinetic energies and the internal energies of the reactants, using (a) independent and (b) and (c) common scaling factors. Dashed lines show the model cross-sections in the absence of experimental energy broadening for reactants with an internal energy of 0 K. In parts (a) and (b), the internal rotors of the ethanol in the $Na^+(NH_3)$ + C_2H_5OH channel are treated as vibrations, whereas in part (c), they are treated as methyl and hydroxy hindered rotors. Fitting parameters are optimized over energy ranges of 0.0–1.8 eV in part (a), 0.0–0.9 eV in part (b), and 0.0–1.2 in part (c).

3.3. Theoretical results

3.3.1. Optimized $L_1Na^+L_2$ geometries

As described above, structures for all the $L_1Na^+L_2$ complexes studied experimentally were calculated at the MP2(full)/6-31G* level of theory. The details of the final optimized geometries are given in Table 5 for all the $L_1Na^+L_2$ complexes and the pictorial representations of several of these structures are displayed in Fig. 6. For the complexes examined, there were several structural minima of essentially equivalent energies (less than 0.1 kJ/mol differences in energy). The primary differences between them are defined by the Y′–X′–X–Y dihedral angles between the two ligands, where X and X′ represent the heavy atoms bound directly to

Table 3
Threshold dissociation energies (in eV) for $LNa^+(C_2H_5OH)$ complexes using independent and common scaling factors and treating the internal rotations of the C_2H_5OH product as vibrations or internal rotors (free and hindered)[a]

	Independent Scaling		Common Scaling									
	Freq[b]		Freq[b]		Free Rotors[c]		CH_3 Hind, OH Free[d]		CH_3 Free, OH Hind[e]		Hindered Rotors[f]	
Ligand	$E_{0,1}$[g]	ΔE_0	$E_{0,1}$[g]	ΔE_0	$E_{0,1}$[g]	ΔE_0	$E_{0,1}$[g]	ΔE_0	$E_{0,1}$[g]	ΔE_0	$E_{0,1}$[g]	ΔE_0
H_2O	0.80	0.257	0.76	0.189	0.77	0.263	0.80	0.234	0.79	0.256	0.80	0.228
C_6H_6	0.84	0.169	0.85	0.107	0.87	0.190	0.85	0.161	0.85	0.184	0.85	0.155
CH_3OH	0.92	0.120	0.85	0.099	0.86	0.168	0.89	0.144	0.89	0.162	0.89	0.139
NH_3	0.92	0.119	0.95	0.047	0.92	0.086	0.93	0.066	0.91	0.077	0.95	0.063

[a] For simplicity, uncertainties in the thresholds are not shown. The uncertainties are equal or comparable to those given in Tables 1 and 2.
[b] Values obtained treating the internal rotors of the ethanol product as vibrations.
[c] Values obtained treating the internal rotors of the ethanol product as free methyl and hydroxy rotors.
[d] Values obtained treating the internal rotors of the ethanol product as a hindered methyl rotor and a free hydroxy rotor.
[e] Values obtained treating the internal rotors of the ethanol product as a free methyl rotor and a hindered hydroxy rotor.
[f] Values obtained treating the internal rotors of the ethanol product as hindered methyl and hydroxy rotors.
[g] Threshold dissociation energy for the first product channel listed in Tables 1 and 2.

Na^+, and Y and Y′ represent the heaviest atoms bound to X and X′, respectively. This indicates that there is free, unhindered rotation about the metal–ligand bond axes. The exceptions to this were the $(H_2O)Na^+(CH_3OH)$, $(H_2O)Na^+(CH_3OCH_3)$, $(H_2O)Na^+(C_2H_5OH)$, $(CH_3OH)Na^+(CH_3OCH_3)$, and $(CH_3OH)Na^+(C_2H_5OH)$ complexes. In these systems, the structural minima for which the Y′–O–O–Y dihedral angle was ∼90° was energetically favored over structures with 0 or 180° dihedral angles by 0.6–0.9 kJ/mol at the MP2(full)/6-31G* level.

For a given complex, the structural details are listed in Table 5 for only one of these optimized geometries, generally the structure with the lowest energy or the highest symmetry for complexes where the ligands are essentially free rotors. In general, the calculations predict that the Na^+–X distances and Na^+–X–Y angles are roughly the same for a single type of ligand, regardless of what second ligand is attached to the sodium cation. For example, all six complexes containing water possess Na^+–O distances between 2.22–2.24 A° and Na^+–O–H angles between 127.6–127.7°. In fact, the Na^+–X distances and Na^+–X–Y angles determined here for the $L_1Na^+L_2$ complexes are also roughly equivalent to those reported by Armentrout and Rodgers [3] for the singly

Table 4
Experimental relative Na^+–L bond dissociation energies at 0 K (in kJ/mol)

	Independent scaling		Common scaling	
Ligand	Freq[a]	Hindered[b]	Freq[a]	Hindered[b]
C_2H_5OH	10.4 (2.3)	6.8 (1.1)	4.7 (0.5)	7.8 (1.2)
NH_3	0.0	0.0	0.0	0.0
CH_3OCH_3	0.4 (1.6)	−0.2 (1.4)	−1.3 (1.1)	−1.6 (1.0)
CH_3OH	−3.4 (2.0)	−4.4 (1.9)	−4.6 (0.8)	−4.9 (1.0)
C_6H_6	−5.8 (1.7)	−6.7 (1.8)	−6.5 (2.0)	−6.9 (2.0)
H_2O	−18.5 (3.2)	−19.6 (2.8)	−14.2 (2.5)	−14.4 (2.7)

[a] Values obtained treating the internal rotors of the ethanol product as vibrations.
[b] Values obtained treating the internal rotors of the ethanol product as hindered methyl and hydroxy rotors.

Table 5
Geometrical parameters of the MP2(full)/6-31G* optimized structures of the $L_1Na^+L_2$ complexes[a]

Complex	Symmetry	Na^+–X Distance (Å)[b]	∠X′Na^+X (°)	∠Na^+XY (°)[b]	∠Y′−X′−X−Y Dihedral Angle (°)
$(H_2O)Na^+(C_6H_6)$	C_{2v}	2.22 (W), 2.77 (B)	180.0[c]	127.6 (W), 75.3 (B)	0.0
$(H_2O)Na^+(CH_3OH)$	C_s	2.24 (W), 2.22 (M)	178.4	127.6 (W), 129.3 (M)	89.4
$(H_2O)Na^+(NH_3)$	C_s	2.24 (W), 2.38 (A)	179.7	127.7 (W), 113.5 (A)	0.0
$(H_2O)Na^+(CH_3OCH_3)$	C_{2v}	2.24 (W), 2.22 (D)	180.0	127.7 (W), 124.6 (D)	90.0
$(H_2O)Na^+(C_2H_5OH)$	C_s	2.24 (W), 2.22 (E)	179.0	127.7 (W), 121.7 (E)	89.6
$(C_6H_6)Na^+(CH_3OH)$	C_s	2.76 (B), 2.21 (M)	180.0[c]	75.3 (B), 128.2 (M)	0.0
$(C_6H_6)Na^+(CH_3OCH_3)$	C_{2v}	2.76 (B), 2.21 (D)	180.0[c]	75.3 (B), 124.6 (D)	0.0
$(C_6H_6)Na^+(NH_3)$	C_{3v}	2.77 (B), 2.37 (A)	180.0[c]	75.4 (B), 113.4 (A)	0.0
$(C_6H_6)Na^+(C_2H_5OH)$	C_s	2.76 (B), 2.21 (E)	180.0[c]	75.3 (B), 120.9 (E)	0.0
$(CH_3OH)Na^+(CH_3OCH_3)$	C_s	2.23 (M), 2.23 (D)	180.0	129.5 (M), 124.6 (D)	90.0
$(CH_3OH)Na^+(NH_3)$	C_s	2.23 (M), 2.38 (A)	179.7	129.6 (M), 113.5 (A)	0.0
$(CH_3OH)Na^+(C_2H_5OH)$	C_1	2.23 (M), 2.22 (E)	178.9	129.0 (M), 121.7 (E)	89.7
$(CH_3OCH_3)Na^+(NH_3)$	C_s	2.22 (D), 2.38 (A)	179.7	124.6 (D), 113.5 (A)	0.0
$(NH_3)Na^+(C_2H_5OH)$	C_s	2.38 (A), 2.22 (E)	176.5	113.6 (A), 122.1 (E)	0.0

[a] X and X′ are the atoms in the two ligands that are closest to the sodium cation; Y and Y′ are the heaviest atoms bonded to X and X′, respectively.
[b] The designations in parenthesis refer to the ligands to which the value applies; W = water, B = benzene, M = methanol, A = ammonia, D = dimethyl ether, E = ethanol.
[c] Angle with respect to the benzene centroid.

ligated Na^+–L complexes with the same ligands, also calculated at the MP2(full)/6-31G* level of theory. This suggests that the binding of the second ligand does not perturb the geometry of the sodium cation with the first ligand to a great extent. For all complexes, except those involving benzene, the X′–Na^+–X angle is nearly linear, with values between 176.5–180.0°. In the benzene complexes, the corresponding angle to the centroid of the ring is also linear. In all cases, the geometry of the ligand when complexed to the sodium cation is very close to the geometry of the free ligand, indicating very little distortion upon complexation.

3.3.2. Calculated L_1Na^+–L_2 bond dissociation energies

As described above, theoretical L_1Na^+–L_2 bond dissociation energies were calculated using the MP2(full)/6-31G* optimized geometries and single-point energy calculations at the MP2(full)/6-311+G(2d,2p) level, corrected for zero-point energies and basis set superposition errors. These values are listed in Table 6 along with the current experimental determinations obtained using the analysis involving common scaling factors and the hindered rotor treatment for both of the internal rotors of ethanol. In addition, calculations were also performed (at the same level as above) to determine the $(CH_3OCH_3)Na^+$–(CH_3OCH_3) and $(H_2O)Na^+$–(H_2O) BDEs, which are available experimentally [16,17], and these values are also listed in Table 6.

4. Discussion

4.1. Relative and absolute Na^+–L bond dissociation energies

Table 4 shows that the various relative BDEs for several of the ligands do not change appreciably no matter which interpretation of the data is used. However, the values for ethanol and water do vary somewhat depending on whether the independent scaling or common scaling approach is used. Independent scaling pushes the relative value for H_2O lower and that for C_2H_5OH higher. Further, dimethyl ether is found to have a slightly higher sodium cation affinity than ammonia when independent scaling is used (and hindered rotors are treated as vibrations), whereas the values are clearly lower when common scaling is used. One qualitative check of the correct affinity

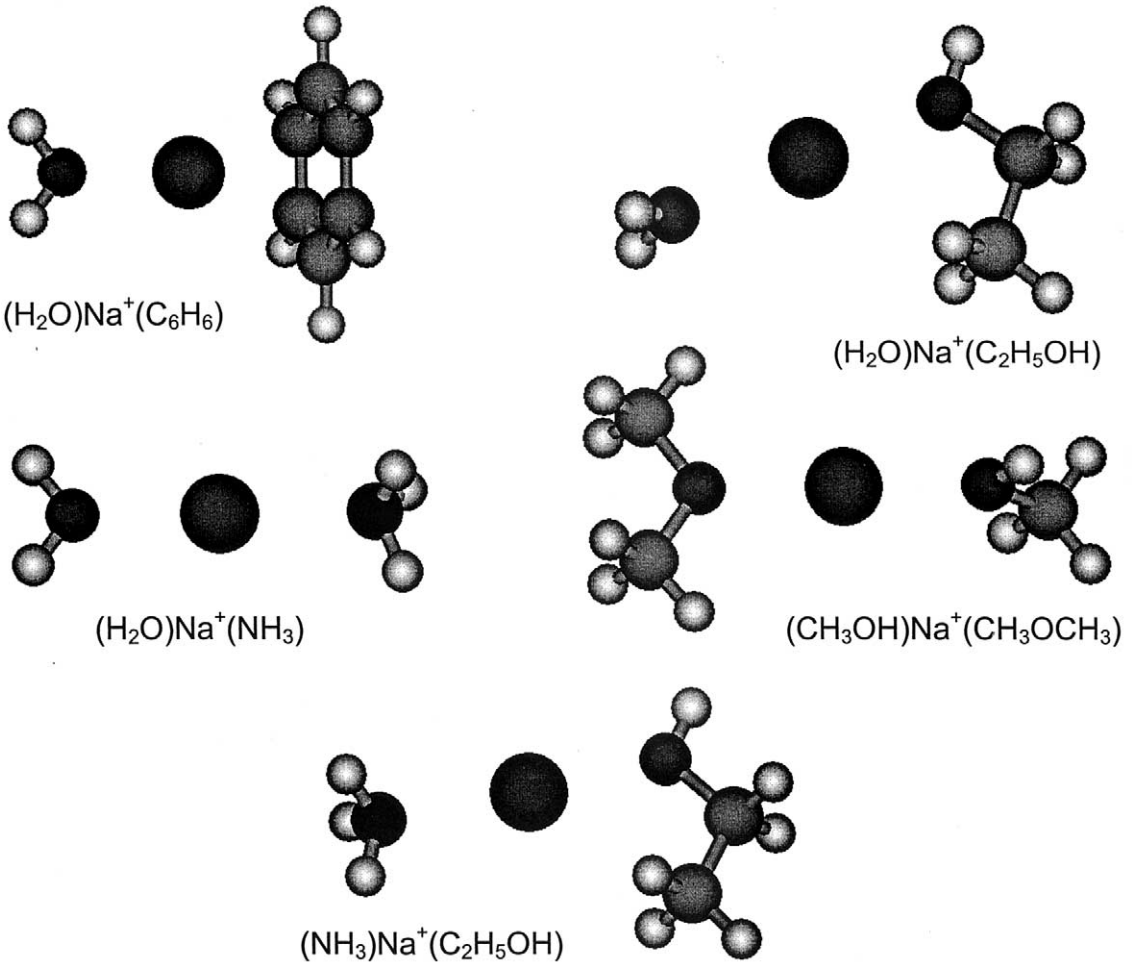

Fig. 6. Ground state geometries of $(H_2O)Na^+(C_6H_6)$, $(H_2O)Na^+(C_2H_5OH)$, $(H_2O)Na^+(NH_3)$, $(CH_3OH)Na^+(CH_3OCH_3)$, and $(NH_3)Na^+(C_2H_5OH)$ complexes, optimized at the MP2(full)/6-31G* level of theory.

ordering comes from the relative apparent thresholds of the low energy $L_1Na^+L_2$ cross sections. This finds the same order as that determined by the analysis using a common scaling factor, i.e. ethanol > ammonia > dimethyl ether > methanol > benzene > water. The method of analysis using a common scaling factor for both channels is the more rigorously correct treatment of the data [23], however, this sometimes does not allow accurate reproduction of the data over as large an energy range as is possible with independent scaling factors. Treating the internal rotations of the ethanol product as rotors largely removes this deficiency for the ethanol complexes. To verify which method of analysis provides the most accurate relative and absolute Na^+–L bond energies, we compare to previously determined literature thermochemistry and theoretical values.

Table 7 lists the absolute Na^+–L bond dissociation energies determined from the current competitive CID experiments where relative values were obtained from Table 4 (columns 3 and 5). Also listed are experimental values determined using pulsed high-pressure mass spectrometry [1], derived from FTICR ligand exchange equilibrium experiments [2], and the absolute CID results previously determined in our laboratory [3]. Fig. 7 compares these various experimental val-

Table 6
Experimental (competitive analysis with common scaling factors and hindered rotor treatment for ethanol) and theoretical bond dissociation energies (in kJ/mol) of L_1Na^+–L_2 at 0 K[a]

	L_2					
L_1	C_2H_5OH	NH_3	CH_3OCH_3	CH_3OH	C_6H_6	H_2O
None	110.0 (5.5)[b]	102.2 (5.4)[b]	100.6 (5.5)[b]	97.3 (5.5)[b]	95.3 (5.7)[b]	87.8 (6.0)[b]
	108.9[c]	*102.5*[c]	*101.7*[c]	*100.0*[c]	*89.4*[c]	*89.2*[c]
C_2H_5OH		91.7 (5.8)		85.9 (6.8)	82.0 (4.8)	77.1 (6.8)
		87.4		*85.4*	*73.3*	*75.8*
NH_3	97.4 (5.8)		86.8 (5.8)	89.7 (6.8)	81.0 (4.8)	83.0 (4.8)
	93.8		*87.4*	*86.3*	*74.0*	*77.1*
CH_3OCH_3		89.7 (5.8)	82.0 (4.8)[d]	85.9 (5.8)	79.1 (4.8)	75.2 (4.8)
		88.2	*87.1*	*86.5*	*74.0*	*76.8*
CH_3OH	99.4 (6.8)	95.5 (6.8)	88.8 (5.8)		81.0 (4.8)	83.0 (5.8)
	94.3	*88.8*	*88.2*		*74.3*	*77.2*
C_6H_6	96.5 (4.8)	89.7 (4.8)	83.9 (4.8)	83.9 (4.8)	80.0 (5.8)[e]	76.2 (5.8)
	92.8	*87.1*	*86.3*	*84.9*	*71.8*[e]	*75.6*
H_2O	99.4 (6.8)	95.5 (4.8)	89.7 (4.8)	93.6 (5.8)	86.8 (5.8)	82.0 (5.8)[f]
	95.5	*90.4*	*89.3*	*88.0*	*75.8*	*78.7*

[a] Uncertainties in parentheses. Ab initio calculated values, MP2(full)/6−311+G(2d,2p)//MP2(full)/6−31G* including ZPE and BSSE corrections, are in italics. Experimental values taken from Table 2.
[b] Values taken from column 4 of Table 7.
[c] See [3].
[d] See [17].
[e] See [20].
[f] See [16].

ues. The FTICR results provide free energies of sodium cation binding to the ligands, which are listed in Table 8. These are converted to the binding enthalpies in Table 7 using enthalpic and entropic correction factors listed in Table 8. The dissociation entropies are calculated with the scaled vibrational frequencies and rotational constants calculated at the MP2(full)/6-31G* level [3]. The enthalpic conversions from 298 to 0 K were determined as described previously [3]. Uncertainties in the calculated entropies and enthalpic conversions were determined by varying the metal-ligand frequencies by a factor of 2 and the frequencies of the ligands by 10%.

For $Na^+(C_2H_5OH)$, the dissociation entropy was calculated using three different treatments of the CH_3 and OH internal rotations of the neutral ethanol product: (a) vibrators, (b) free rotors, and (c) hindered rotors. This resulted in ΔS values of 94.4, 114.9, and 107.6 J/K mol, respectively. Using the literature ΔG_{298} value for $Na^+(C_2H_5OH)$ dissociation (79.5 kJ/mol) [2], ΔH_{298} values of 107.6, 113.7, and 111.6 kJ/mol, respectively, were obtained. The 298 to 0 K enthalpy corrections were explicitly calculated for the vibrator and free rotor treatments as 1.3 and 1.6 kJ/mol, respectively, whereas the average of these values, 1.4 kJ/mol, was used for the hindered rotor treatment. These corrections yield ΔH_0 values of 106.3, 112.1, and 110.1 kJ/mol, respectively. Because the hindered rotor treatment was determined to be the best method of analyzing the data with a common scaling factor for the systems with ethanol, the ΔH_0 value presented in Table 7 is that derived using this method to calculate the entropic and enthalpic corrections. Note that this treatment has a nonnegligible affect on the conversion between free energies at 298 K and enthalpies at 0 K.

As can be seen from Table 7 and Fig. 7, the best quantitative agreement between the present competitive CID results and the literature thermochemistry is obtained when the data are analyzed using a common scaling factor [mean absolute deviation (MAD) of 0.9 ± 0.5 kJ/mol; eight values]. Also note that the relative ordering (specifically the NH_3 vs. CH_3OCH_3 values) is the same for these two data sets. Values obtained

Table 7
Experimental and theoretical absolute Na^+–L bond dissociation energies at 0 K (in kJ/mol) and mean absolute deviations (MADs)

	Experiment				Theory[a]			
Ligand	CID[a]	CCID I.S.[b]	CCID C.S.[c]	Literature[d]	MP2	G2	CBS-Q	B3LYP
C_2H_5OH	102.0 (3.7)	109.0 (5.5)	110.0 (5.5)	110.1 (5.1)[e]	108.9	107.6	104.4	114.7
NH_3	102.2 (5.4)	102.2 (5.4)	102.2 (5.4)	102.6 (4.0) 103.1 (0.8)[f]	102.5	102.2	96.7	108.7
CH_3OCH_3	91.7 (4.8)	102.0 (5.6)	100.6 (5.5)	99.6 (5.1)	101.7	100.3	101.0	105.5
CH_3OH	91.7 (5.7)	97.8 (5.7)	97.3 (5.5)	97.9 (5.0) 98.9 (0.8)[f]	100.0	98.5	96.2	105.2
C_6H_6	88.3 (4.3) 92.6 (5.8)[g]	95.5 (5.7)	95.3 (5.7)	94.5 (4.4)	89.4	94.4	90.9	94.9
H_2O	94.6 (7.5)	82.6 (6.1)	87.8 (6.0)	89.4 (5.2)	89.2	88.8	88.8	94.6
Direct CID[h]	0.0	6.5 (4.1)	5.6 (3.2)	4.9 (3.0)	5.0 (3.6)	5.0 (3.0)	4.5 (2.6)	7.9 (5.6)
CCID I.S.[i]	6.5 (4.1)	0.0	1.4 (1.9)	1.7 (2.2)	2.6 (3.0)	1.8 (2.2)	3.9 (2.1)	6.0 (3.8)
CCID C.S.[j]	5.6 (3.2)	1.4 (1.9)	0.0	0.9 (0.5)	2.1 (2.0)	1.0 (0.8)	3.0 (2.4)	5.2 (2.6)
Literature[k]	4.9 (3.0)	1.7 (2.2)	0.9 (0.5)	0.0	1.6 (1.6)	0.8 (0.7)	3.5 (2.2)	5.2 (2.1)

[a] See [3]; MP2 = MP2 (full)/6-311+G(2d,2p)//MP2(full)/6-31G*, B3LYP = B3LYP/6-311+G(2d,2p)//B3LYP/6-31G*.
[b] Present $L_1Na^+L_2$ competitive CID results with independent scaling factors and hindered rotors for the ethanol product. Values taken from column 3 of Table 4.
[c] Present $L_1Na^+L_2$ competitive CID results with common scaling factors and hindered rotors for the ethanol product. Values taken from column 5 of Table 4.
[d] Calculated from experimental ΔG_{298} values reported by McMahon & Ohanessian [2] and enthalpy and entropy corrections determined at the MP2(full)/6-31G* level [3].
[e] Entropy correction calculated using the hindered rotor treatment for the neutral ethanol internal rotors as described in the text.
[f] See [1].
[g] See [20].
[h] Mean absolute deviation from direct CID results.
[i] Mean absolute deviation from competitive CID results with independent scaling factors.
[j] Mean absolute deviation from competitive CID results with common scaling factors.
[k] Mean absolute deviation from literature values.

from the competitive CID analysis using independent scaling factors have a larger MAD (1.7 ± 2.2 kJ/mol; eight values). It is reasonable to ask whether our assignment of 102.2 kJ/mol for the absolute anchor influences this agreement. We can evaluate this simply by asking what the best anchor value would be to minimize the discrepancies on a statistical basis, i.e. minimize $\Sigma[SIA(NH_3) + SIA(L,rel) - SIA(L,Lit)]^2$ where the summation is over all ligands, SIA is the sodium ion affinity, rel is for the relative values in Table 4, and Lit is for the literature values from [1,2]. The optimum value for $SIA(NH_3)$ is found to be 102.6 ± 1.0 kJ/mol, in excellent agreement with our direct CID measurement.

The BDEs previously determined in our laboratory using direct Na^+–L CID experiments are also within experimental error of the literature values (MAD of 4.9 ± 3.0 kJ/mol; nine values), but the order is different (specifically with regard to the H_2O ligand), although not outside combined experimental errors. Interestingly, comparison of our previous absolute CID results for Na^+–L also find that deviations are minimized when the present data are analyzed using a common scaling factor (MAD of 5.6 ± 3.2 kJ/mol; seven values) versus independent scaling factors (MAD of 6.5 ± 4.1 kJ/mol; seven values). Optimum agreement between our present relative values and the previous direct CID values would be obtained using an anchor value of $SIA(NH_3)$ = 98.6 ± 5.6 kJ/mol, somewhat lower than the chosen value but well within the associated uncertainties.

To this point, we have relied on a comparison with

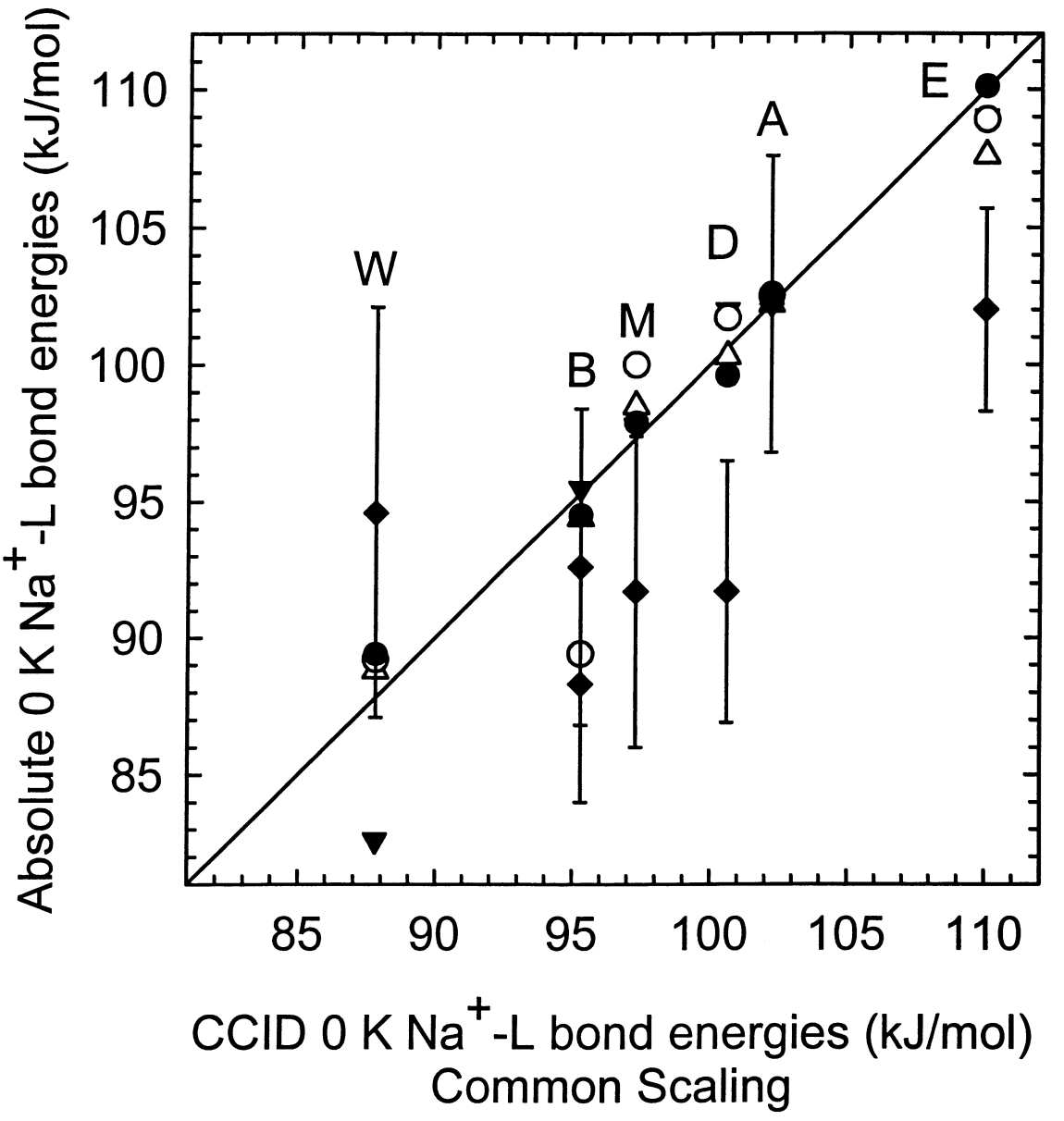

Fig. 7. Absolute 0 K Na^+–L bond dissociation energies determined by direct CID (closed diamonds with error bars [3,20]), competitive CID with independent scaling factors (closed inverted triangles, present work), FTICR equilibrium studies (closed circles [2]), and theoretical calculations at the MP2(full)/6-311+G(2d,2p)//MP2(full)/6-31G* level (open circles [3]) and using the G2 composite method (open triangles [3]) vs. competitive CID (CCID) with a common scaling factor. All values are listed in Table 7. The diagonal line indicates the values for which direct CID, competitive CID with independent scaling, FTICR and theory values are equal to the competitive CID values with a common scaling factor. The designations W, B, M, D, A, and E refer to water, benzene, methanol, dimethyl ether, ammonia, and ethanol, respectively.

experimental literature values to assess the best relative and absolute sodium ion affinities. Unfortunately, this relies on accurate transformations of free energy data to 0 K enthalpies, a process that can be flawed by some of the same limitations as our statistical fitting procedure. Alternatively, we can compare to sets of 0

Table 8
Enthalpies and free energies (in kJ/mol) for Na^+–L at 0 and 298 K[a]

Ligand	ΔH_0[b]	$\Delta H_{298}-\Delta H_0$[c]	ΔH_{298}	$T\Delta S_{298}$[c]	ΔG_{298}	ΔG_{298} (lit)[d]
C_2H_5OH	110.0 (5.5)	1.4 (1.3)[e]	111.4 (5.6)	32.1 (4.8)[e]	79.3 (7.7)	79.5 (0.9)
NH_3	102.2 (5.4)	4.0 (1.8)	106.2 (5.7)	28.8 (3.4)	77.4 (6.6)	77.8 (1.1)
CH_3OCH_3	100.6 (5.5)	0.8 (1.3)	101.4 (5.6)	26.8 (4.8)	74.6 (7.4)	73.6 (1.2)
CH_3OH	97.3 (5.5)	1.5 (1.4)	98.8 (5.7)	27.0 (4.7)	71.8 (7.4)	72.4 (1.2)
C_6H_6	95.3 (5.7)	1.7 (1.5)	97.0 (5.9)	30.5 (4.8)	66.5 (7.6)	65.7 (1.4)
H_2O	87.8 (6.0)	3.4 (1.9)	91.2 (6.3)	27.1 (3.8)	64.1 (7.4)	65.7 (1.4)

[a] Uncertainties in parenthesis.
[b] Present experimental results (column 4 of Table 7).
[c] Calculated using standard formulas and molecular constants determined at the MP2(full)/6-31G* level [3]. Uncertainties correspond to increases and decreases in the metal-ligand frequencies by a factor of 2 and ±10% variations in the ligand frequencies.
[d] See [2].
[e] Calculated using hindered rotor treatment for neutral ethanol internal rotations as described in the text.

K BDEs calculated at several levels of theory. Armentrout and Rodgers [3] assessed a number of theoretical treatments for the complexes of interest here. In this work, we compare to theoretical values calculated at two values commonly used in the literature: MP2(full)/6-311+G(2d,2p)//MP2(full)/6-31G* and B3LYP/6-311+G(2d,2p)//B3LYP/6-31G* levels (both including zero point energy and basis set superposition error corrections). We also compare to the composite methods designed to produce high accuracy thermochemistry, G2 [67] and CBS-Q [68]. The values are all taken from [3] and are listed in Table 7. Comparison of the direct CID and competitive CID results (independent and common scaling) to the theoretical BDEs shows that the best agreement is obtained with the common scaling factor results (see MAD values in Table 7). It is also useful to determine the optimum value for the anchor, SIA(NH_3), for the common scaling results: 102.0 ± 3.0 kJ/mol for MP2, 102.0 ± 1.3 kJ/mol for G2, 99.7 ± 3.0 kJ/mol for CBS-Q, and 107.3 ± 2.9 kJ/mol for B3LYP. Clearly, discrepancies between experiment and the B3LYP results appear to be because this level of theory systematically overestimates the sodium binding affinities, as previously concluded [3]. These optimum SIA values also reaffirm our choice of 102.2 kJ/mol as a reliable result for the sodium ion affinity of ammonia. As a conservative estimate, we retain the absolute uncertainty (one standard deviation) of 5.4 kJ/mol determined in our CID work although a smaller uncertainty could be warranted. This is propagated to the uncertainties listed in Table 7 for the remaining ligands.

Overall, we believe our best absolute Na^+–L BDEs are the values determined from the present competitive CID experiments in which the data are analyzed using a common scaling factor (column 4 of Table 7). DeTuri and Ervin also concluded that competitive CID data are best analyzed using a common scaling factor in their study of the gas-phase acidities of a number of alcohols [65]. In addition, it is clear that the treatment of the internal rotors of the ethanol product is an influential factor in allowing analysis with common scaling factors over an extended energy range. Although the present results refine the absolute Na^+–L BDEs previously determined in our laboratory, it is important to note that these refined values are not significantly different than those determined by direct CID of Na^+L complexes [3]. In all cases, the differences between the current and previous results are within the combined uncertainties of the two measurements. However, each direct CID study is a completely independent measurement of the absolute Na^+–L BDEs. Determinations of differences between systems with similar absolute BDEs are made much more reliably by equilibrium or competitive CID experiments in which the relative binding is determined directly. In the

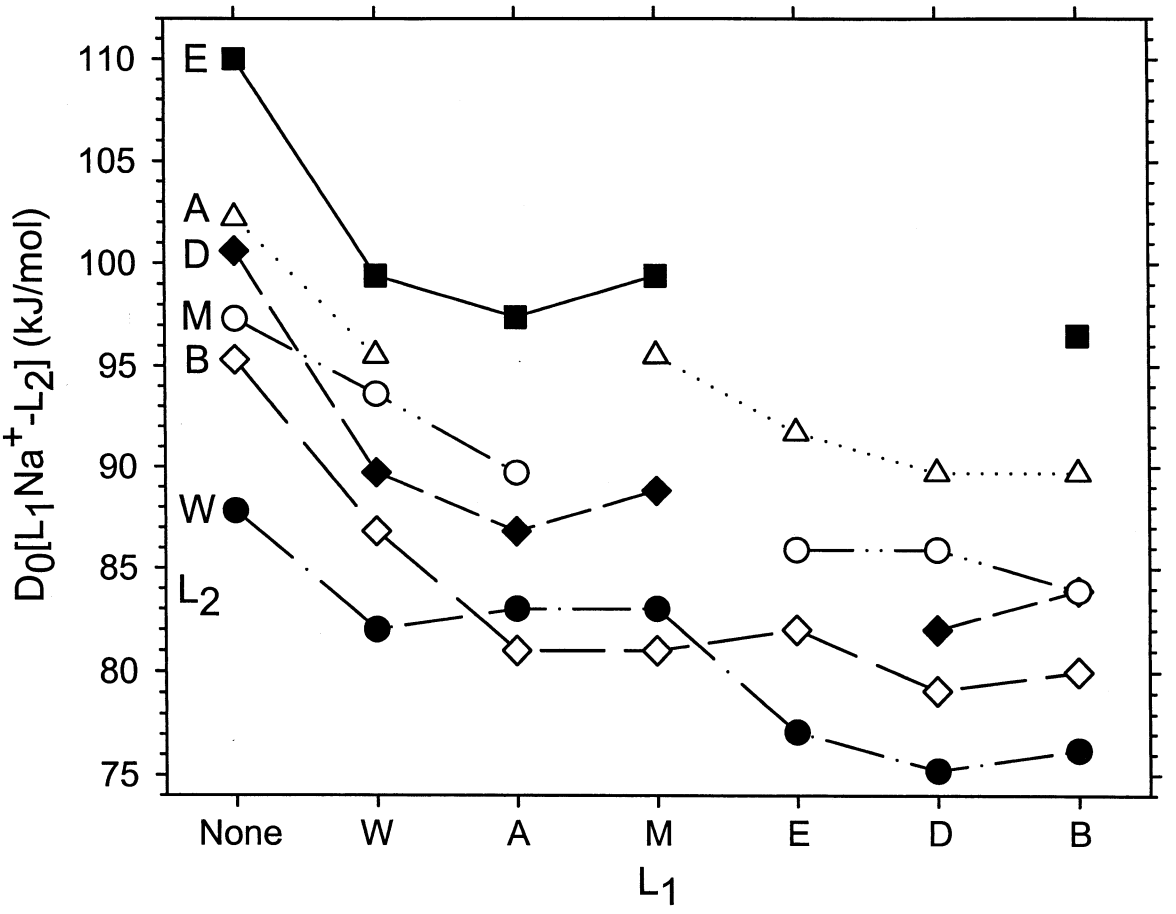

Fig. 8. Absolute 0 K L_1Na^+–L_2 bond dissociation energies as a function of increasing polarizability of the L_1 ligand [69,70], where L_2 = water (W, closed circles), benzene (B, open diamonds), methanol (M, open circles), dimethyl ether (D, closed diamonds), ammonia (A, open triangles), and ethanol (E, closed squares). All bond energies are taken from Table 6.

cases included in this work, for example, the bond energies span a range of only 20 kJ/mol (0.2 eV).

In order to facilitate comparison of our new recommended absolute Na^+–L binding energies determined using competitive CID to other experiments, we have converted our 0 K values to 298 K enthalpies and free energies. These are given in Table 8 along with the absolute free energies determined using FTICR ligand exchange equilibrium experiments [2]. The agreement between the free energies derived from our competitive CID experiments with those determined from the FTICR experiments (MAD of 0.8 ± 0.5) is excellent.

4.3. Absolute L_1Na^+–L_2 bond dissociation energies

As mentioned above, the thresholds measured in the present experiments directly yield the absolute second ligand BDEs to the sodium cation, L_1Na^+–L_2. These values, determined from the data analysis using a common scaling factor, are listed in Table 6 and shown in Fig. 8. Table 6 also includes theoretical values calculated at the MP2(full)/6-311+G(2d,2p)//MP2(full)/6-31G* level of theory including ZPE and BSSE corrections. For all systems studied, the second ligand is more weakly bound to the sodium cation than the first ligand, as expected for the electrostatic

nature of the bonding in these complexes. When the second bond energies are plotted in the order of increasing polarizability for the L_1 ligand [69,70], Fig. 8, it is clear that the second ligand bond energies generally decrease. This is an indication that the extent of electron donation to the metal ion is largest for the more polarizable ligands. Such electron donation decreases the effective nuclear charge on the metal ion and therefore decreases the bond energy for the second ligand. Analogous behavior was observed for the $(R_1OH)Li^+$–(R_2OH) complexes [23].

The agreement between experiment and theory for these sodium cation complexes is generally quite good, with a MAD of 3.6 ± 2.7 kJ/mol (37 values). We also note that the agreement between experiment and MP2 theory when independent scaling factors are used is slightly worse (MAD of 4.9 ± 3.6 kJ/mol, 37 values) than that observed with a common scaling factor. This is further evidence that the analysis using a common scaling factor is the most accurate method of determining thresholds for systems in which competition is occurring. The comparison between experiment and theory is also represented in Fig. 9, where it can be seen that most of the points are evenly scattered about the diagonal line, which represents equivalent experimental and calculated values. The largest systematic exceptions are values for which the second ligand is benzene, i.e. L_1Na^+–(C_6H_6). Without including these systems, the comparison between the other 30 experimental and theoretical values improves to a MAD of 2.7 ± 2.0 kJ/mol. For the benzene systems, the calculated values are low compared to experiment (MAD = 7.5 ± 2.0 kJ/mol, seven values). Given that a comparable deviation (5.9 kJ/mol) is found for the $Na^+(C_6H_6)$ complex (Table 7), this result suggests that the MP2 calculations are slightly inadequate at representing the bonding of Na^+ to the diffuse π cloud of benzene. For the other ligands, this level of theory appears to be adequate for the accurate prediction of the bonding energies of the bis-ligated Na^+ complexes. This is further suggested by comparison between MP2 and G2 theory results for the mono-ligated Na^+ complexes, which agree within 1.0 ± 0.5 kJ/mol (and G2 theory is systematically lower) except for C_6H_6 where G2 results are 5.0 kJ/mol higher. Again this suggests that MP2 calculations for the benzene ligand are low by approximately 6 kJ/mol. Part of the deviation in the MP2 results could be a result of overestimating the BSSE of complexes involving benzene. Specifically, the average BSSE for the benzene containing bis-ligated complexes is 18.1 ± 1.5 kJ/mol, whereas the average BSSE for all other bis-ligated complexes is 12.8 ± 1.2 kJ/mol. The difference of 5.3 kJ/mol is comparable to the shift observed for the G2 vs MP2 results for $Na^+(C_6H_6)$.

5. Conclusions

The binding energies of Na^+ to H_2O, C_6H_6, CH_3OH, CH_3OCH_3, NH_3, and C_2H_5OH cover a range of only 20 kJ/mol, such that equilibrium or competitive experiments are needed to provide precise determinations of the relative bond energies. In the present work, collision-induced dissociation experiments of bis-ligated $L_1Na^+L_2$ complexes, where L_1 and L_2 are these six ligands, with xenon have been performed using a tandem guided ion beam mass spectrometer. The competitive dissociation channels have been simultaneously analyzed to yield absolute L_1Na^+–L_2 and relative Na^+–L bond dissociation energies at 0 K. From the relative Na^+–L binding affinities and the use of an absolute anchor, $D_0[Na^+$–$NH_3]$ determined from direct CID experiments in our laboratory, the absolute Na^+–L binding energies for these ligands could be obtained. Two methods of data analysis were used, independent scaling factors for each channel or a common scaling factor, such that the relative cross section magnitudes are predicted solely by the statistical rate constants. In addition, we found that the internal rotors of the ethanol product need to be treated as hindered rotors rather than vibrators to provide reasonable reproduction of the data using a common scaling factor. The results determined using a common scaling factor were found to give the best agreement with previous results from the literature, both experimental and theoretical. The single ligand binding affinities with the sodium cation, Na^+–L, were found to have the order: ethanol > ammonia >

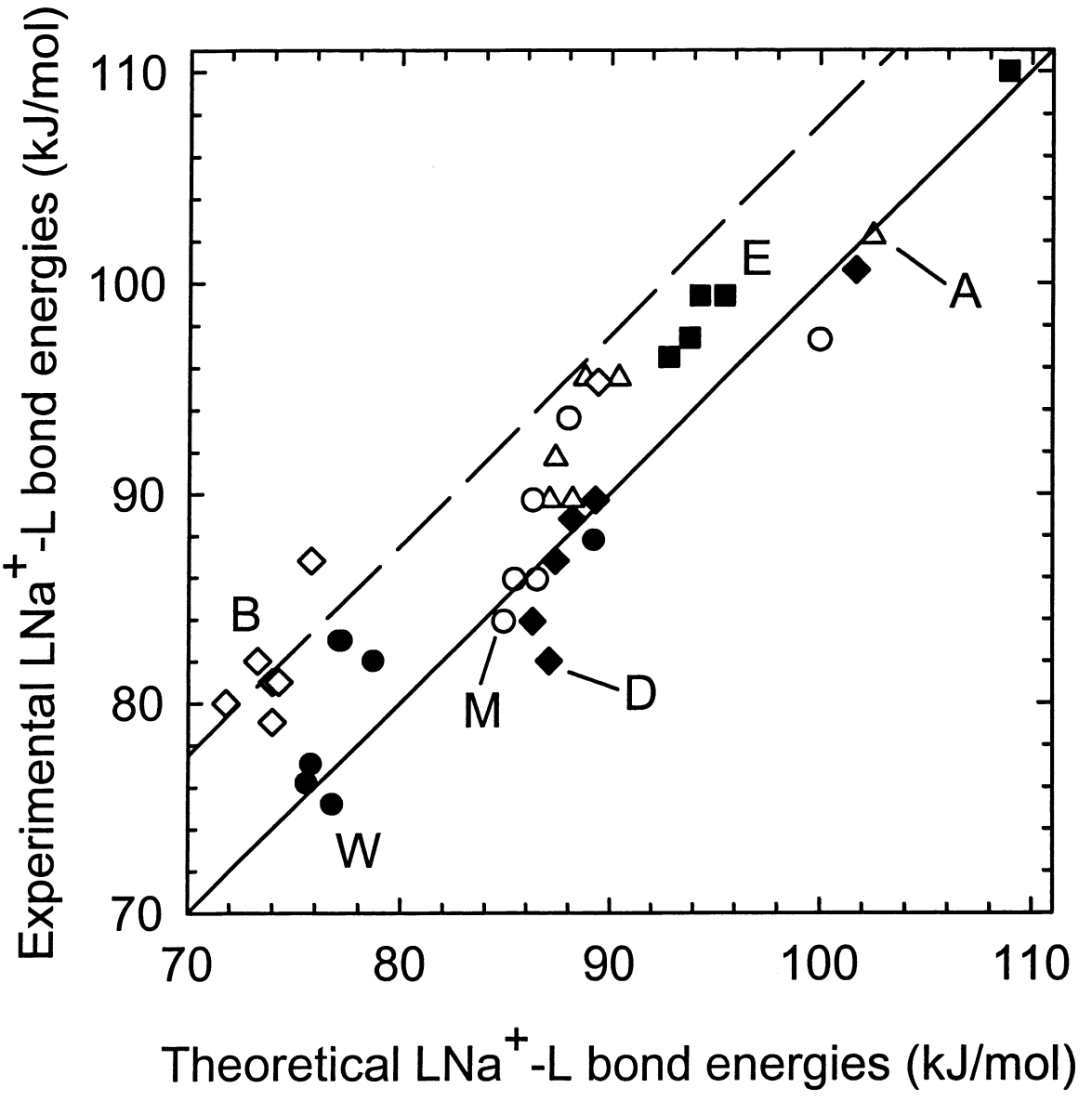

Fig. 9. Experimental vs. theoretical absolute 0 K $L_1Na^+–L_2$ bond dissociation energies, according to the L_2 ligand: water (W, closed circles), benzene (B, open diamonds), methanol (M, open circles), dimethyl ether (D, closed diamonds), ammonia (A, open triangles), and ethanol (E, closed squares). All values are taken from Table 6. The diagonal line indicates the values for which measured and calculated values are equal, whereas the dashed line represents an offset of 7.5 kJ/mol.

dimethyl ether > methanol > benzene > water. The $L_1Na^+–L_2$ bond energies were also calculated using ab initio methods at the MP2(full)/6-311+G(2d,2p)// MP2(full)/6-31G* level and are generally found to be in good agreement with the experimental values. It appears, however, that these MP2 calculations systematically underestimate the binding of benzene to Na^+ by approximately 7 ± 2 kJ/mol. In all cases, the experimental second ligand bond energies are weaker than the first, and these second BDEs exhibit syner-

gistic effects that correlate approximately with the polarizability of the first ligand.

Acknowledgements

Funding for this work was provided by the National Science Foundation under Grant CHE-9877162. The authors thank Kent Ervin and Vince DeTuri for providing us with the least squares minimization program and for valuable discussion concerning hindered rotors. J. A. thanks Rohana Liyanage, Hideya Koizumi, and Felician Muntean for enlightening discussion regarding this work.

References

[1] S. Hoyau, K. Norrman, T.B. McMahon, G. Ohanessian, J. Am. Chem. Soc. 121 (1999) 8864.
[2] T.B. McMahon, G. Ohanessian, Chem. Eur. J. 6 (2000) 2931.
[3] P.B. Armentrout, M.T. Rodgers, J. Phys. Chem. A 104 (2000) 2238.
[4] M.T. Rodgers, P.B. Armentrout, Mass Spectrom. Rev. 19 (2000) 215.
[5] S.J. Lippard, J.M. Berg, Principles of Bioinorganic Chemistry, University Science Books, Mill Valley, CA, 1994.
[6] For example, see P.C. Liao, J. Allison, J. Mass Spectrom. 30 (1995) 408.
[7] A.W. Castleman, Jr., P.M. Holland, D.M. Lindsay, K.I. Peterson, J. Am. Chem. Soc. 100 (1978) 6039.
[8] A.W. Castleman, Jr., K.I. Peterson, B.L. Upschulte, F.J. Schelling, Int. J. Mass Spectrom. Ion Processes 47 (1983) 203.
[9] B.C. Guo, B.J. Conklin, A.W. Castleman, Jr., J. Am. Chem. Soc. 111 (1989) 6506.
[10] B.C. Guo, J.W. Purnell, A.W. Castleman, Jr., Chem. Phys. Lett. 168 (1990) 155.
[11] J.J. Gilligan, L.R. McCunn, B.D. Leskiw, Z. Herman, A.W. Castleman, Jr., Int. J. Mass Spectrom. 204 (2001) 247.
[12] R. Amunugama, M.T. Rodgers, Int. J. Mass Spectrom. 195/196 (2000) 439.
[13] M.T. Rodgers, J. Phys. Chem. A 105 (2001) 2374.
[14] R. Amunugama, M.T. Rodgers, J. Phys. Chem. A, accepted for publication.
[15] M.T. Rodgers, J. Phys. Chem. A, accepted for publication.
[16] N.F. Dalleska, B.L. Tjelta, P.B. Armentrout, J. Phys. Chem. 98 (1994) 4191.
[17] M.B. More, D. Ray, P.B. Armentrout, J. Phys. Chem. A 101 (1997) 831.
[18] D. Walter, M.R. Sievers, P.B. Armentrout, Int. J. Mass Spectrom. Ion Processes 175 (1998) 93.
[19] M.T. Rodgers, P.B. Armentrout, J. Phys. Chem. A 103 (1999) 4955.
[20] J.C. Amicangelo, P.B. Armentrout, J. Phys. Chem. A 104 (2000) 11420.
[21] I. Dzidic, P. Kebarle, J. Phys. Chem. 74 (1970) 1466.
[22] As described below, the free energies from the FTICR experiments were converted to binding enthalpies using entropies calculated from ab initio determined molecular parameters.
[23] M.T. Rodgers, P.B. Armentrout, J. Chem. Phys. 109 (1998) 1787.
[24] K.M. Ervin, P.B. Armentrout, J. Chem. Phys. 83 (1985) 166.
[25] R.H. Schultz, P.B. Armentrout, Int. J. Mass Spectrom. Ion Processes 107 (1991) 29.
[26] F. Muntean, P.B. Armentrout, J. Chem. Phys., 115 (2001) 1213.
[27] E. Teloy, D. Gerlich, Chem. Phys. 4 (1974) 417.
[28] D. Gerlich, in State-Selected and State-to-State Ion-Molecule Reaction Dynamics, Part 1: Experiment, C. Y. Ng, M. Baer (Eds.), Wiley & Sons Inc., New York, 1992, Vol. LXXXII, pp.1–176.
[29] S.K. Loh, L. Lian, D.A. Hales, P.B. Armentrout, J. Chem. Phys. 89 (1988) 3378.
[30] R.H. Schultz, K.C. Crellin, P.B. Armentrout, J. Am. Chem. Soc. 113 (1991) 8590.
[31] N.F. Dalleska, K. Honma, L.S. Sunderlin, P.B. Armentrout, J. Am. Chem. Soc. 116 (1994) 3519.
[32] N.F. Dalleska, K. Honma, P.B. Armentrout, J. Am. Chem. Soc. 115 (1993) 12125.
[33] F.A. Khan, D.E. Clemmer, R.H. Schultz, P.B. Armentrout, J. Phys. Chem. 97 (1993) 7978.
[34] R.H. Schultz, P.B. Armentrout, J. Chem. Phys. 96 (1992) 1046.
[35] E.R. Fisher, B.L. Kickel, P.B. Armentrout, J. Phys. Chem. 97 (1993) 10204.
[36] R.G. Gilbert, S.C. Smith, Theory of Unimolecular and Recombination Reactions, Blackwell Scientific, Oxford, 1990.
[37] D.G. Truhlar, B.C. Garrett, S.J. Klippenstein, J. Phys. Chem. 100 (1996) 12771.
[38] K.A. Holbrook, M.J. Pilling, S.H. Robertson, Unimolecular Reactions, 2nd ed., Wiley, New York, 1996.
[39] J.A. Pople, H.B. Schlegel, K. Raghavachari, D.J. DeFrees, J.F. Binkley, M.J. Frisch, R.F. Whitesides, R.F. Hout, W.J. Hehre, Int. J. Quantum Chem Symp. 15 (1981) 269.
[40] D.J. DeFrees, A.D. McLean, J. Chem. Phys. 82 (1985) 333.
[41] T.S. Beyer, D.F. Swinehart, Commun. Assoc. Comput. Machines 16 (1973) 379.
[42] S.E. Stein, B.S. Rabinovich, J. Chem. Phys. 58 (1973) 2438.
[43] S.E. Stein, B.S. Rabinovich, Chem. Phys. Lett. 49 (1977) 1883.
[44] M.T. Rodgers, P.B. Armentrout, J. Phys. Chem. A 101 (1997) 2614.
[45] M.T. Rodgers, K.M. Ervin, P.B. Armentrout, J. Chem. Phys. 106 (1997) 4499.
[46] E.V. Waage, B.S. Rabinovitch, Chem. Rev. 70 (1970) 377.
[47] W.J. Chesnavich, M.T. Bowers, J. Phys. Chem. 83 (1979) 900.
[48] P.B. Armentrout, in Advances in Gas Phase Ion Chemistry, N. G. Adams, L. M. Babcock (Eds.), JAI Press Inc., Greenwich, CT, 1992, Vol. 1, pp. 83–119.

[49] M.B. More, E.D. Glendening, D. Ray, D. Feller, P.B. Armentrout, J. Phys. Chem. 100 (1996) 1605.
[50] D. Ray, D. Feller, M.B. More, E.D. Glendening, P.B. Armentrout, J. Phys. Chem. 100 (1996) 16116.
[51] M.T. Rodgers, P.B. Armentrout, J. Phys. Chem. A 101 (1997) 1238.
[52] M.B. More, D. Ray, P.B. Armentrout, J. Phys. Chem. A 101 (1997) 4254.
[53] M.B. More, D. Ray, P.B. Armentrout, J. Phys. Chem. A 101 (1997) 7007.
[54] N.F. Dalleska, K. Honma, P.B. Armentrout, J. Am. Chem. Soc. 115 (1993) 12125.
[55] P.B. Armentrout, J. Simons, J. Am. Chem. Soc. 114 (1992) 8627.
[56] M.J. Frisch, G.W. Trucks, H.B. Schlegel, G.E. Scuseria, M.A. Robb, J.R. Cheeseman, V.G. Zakrzewski, J.A. Montgomery, Jr., R.E. Stratmann, J.C. Burant, S. Dapprich, J.M. Millam, A.D. Daniels, K.N. Kundin, M.C. Strain, O. Farkas, J. Tomasi, V. Barone, M. Cossi, R. Cammi, B. Mennucci, C. Pomelli, C. Adamo, S. Clifford, J. Ochterski, G.A. Petersson, P.Y. Ayala, Q. Cui, K. Morokuma, D.K. Malick, A.D. Rabuck, K. Raghavachari, J.B. Foresman, J. Cioslowski, J.V. Ortiz, B.B. Stefanov, G. Liu, A. Liashenko, P. Piskorz, I. Komaromi, R. Gomperts, R.L. Martin, D.J. Fox, T. Keith, M.A. Al-Laham, C.Y. Peng, A. Nanayakkara, C. Gonzalez, M. Challacombe, P.M.W. Gill, B. Johnson, W. Chen, M.W. Wong, J.L. Andres, C. Gonzalez, M. Head-Gordon, E.S. Replogle, J.A. Pople, GAUSSIAN 98, Revision A.7, Gaussian, Inc., Pittsburgh, PA, 1998.
[57] J.B. Foresman, A.E. Frisch, Exploring Chemistry with Electronic Structure Methods, 2nd ed., Gaussian, Inc., Pittsburgh, PA, 1996.
[58] S.F. Boys, R. Bernardi, Mol. Phys. 19 (1970) 553.
[59] F.B. van Duijneveldt, J.G.C.M. van Duijneveldt-van de Rijdt, J.H. van Lenthe, Chem. Rev. 94 (1994) 1873.
[60] J.C. Amicangelo, P.B. Armentrout, unpublished results for CID of doubly ligated complexes of the sodium ion where the ligands are alcohols.
[61] R.G. Cooks, J.T. Patrick, T. Kotiaho, S.A. McLuckey, Mass Spectrom. Rev. 13 (1994) 287.
[62] R.G. Cooks, P.H. Wong, Acc. Chem. Res. 31 (1998) 379.
[63] R.G. Cooks, J.T. Koskinen, P.D. Thomas, J. Mass Spectrom. 34 (1999) 85.
[64] P.B. Armentrout, J. Mass Spectrom. 34 (1999) 74.
[65] V.F. DeTuri, K.M. Ervin, J. Phys. Chem. A 103 (1999) 6911.
[66] J. Chao, K.R. Hall, K.N. Marsh, R.C. Wilhoit, J. Phys. Chem. Ref. Data 15 (1986) 1369.
[67] L.A. Curtiss, K. Raghavachari, G.W. Trucks, J.A. Pople, J. Chem. Phys. 94 (1991) 7221.
[68] J.W. Ochterski, G.A. Petersson, J.A. Montgomery, J. Chem. Phys. 104 (1996) 2598.
[69] E.W. Rothe, R.B. Bernstein, J. Chem. Phys. 31 (1959) 1619.
[70] J. Applequist, J.R. Carl, K.K. Fung, J. Am. Chem. Soc. 94 (1972) 2952.